PTEP

Prog. Theor. Exp. Phys. **2015**, 043C01 (36 pages)
DOI: 10.1093/ptep/ptv031

Neutrino oscillation physics potential of the T2K experiment

The T2K Collaboration

K. Abe[1], J. Adam[2], H. Aihara[3,4], T. Akiri[5], C. Andreopoulos[6], S. Aoki[7], A. Ariga[8], S. Assylbekov[9], D. Autiero[10], M. Barbi[11], G.J. Barker[12], G. Barr[13], P. Bartet-Friburg[14], M. Bass[9], M. Batkiewicz[15], F. Bay[16], V. Berardi[17], B.E. Berger[4,9], S. Berkman[18], S. Bhadra[19], F.d.M. Blaszczyk[20], A. Blondel[21], C. Bojechko[22], S. Bordoni[23], S.B. Boyd[12], D. Brailsford[24], A. Bravar[21], C. Bronner[4], N. Buchanan[9], R.G. Calland[25], J. Caravaca Rodríguez[23], S.L. Cartwright[26], R. Castillo[23], M.G. Catanesi[17], A. Cervera[27], D. Cherdack[9], G. Christodoulou[25], A. Clifton[9], J. Coleman[25], S.J. Coleman[28], G. Collazuol[29], K. Connolly[30], L. Cremonesi[31], A. Dabrowska[15], I. Danko[32], R. Das[9], S. Davis[30], P. de Perio[33], G. De Rosa[34], T. Dealtry[6,13], S.R. Dennis[6,12], C. Densham[6], D. Dewhurst[13], F. Di Lodovico[31], S. Di Luise[16], O. Drapier[35], T. Duboyski[31], K. Duffy[13], J. Dumarchez[14], S. Dytman[32], M. Dziewiecki[36], S. Emery-Schrenk[37], A. Ereditato[8], L. Escudero[27], T. Feusels[18], A.J. Finch[38], G.A. Fiorentini[19], M. Friend[39,†], Y. Fujii[39,†], Y. Fukuda[40], A.P. Furmanski[12], V. Galymov[10], A. Garcia[23], S. Giffin[11], C. Giganti[14], K. Gilje[2], D. Goeldi[8], T. Golan[41], M. Gonin[35], N. Grant[38], D. Gudin[42], D.R. Hadley[12], L. Haegel[21], A. Haesler[21], M.D. Haigh[12], P. Hamilton[24], D. Hansen[32], T. Hara[7], M. Hartz[4,43], T. Hasegawa[39,†], N.C. Hastings[11], T. Hayashino[44], Y. Hayato[1,4], C. Hearty[18,‡], R.L. Helmer[43], M. Hierholzer[8], J. Hignight[2], A. Hillairet[22], A. Himmel[5], T. Hiraki[44], S. Hirota[44], J. Holeczek[45], S. Horikawa[16], K. Huang[44], A.K. Ichikawa[44,*], K. Ieki[44], M. Ieva[23], M. Ikeda[1], J. Imber[2], J. Insler[20], T.J. Irvine[46], T. Ishida[39,†], T. Ishii[39,†], E. Iwai[39], K. Iwamoto[47], K. Iyogi[1], A. Izmaylov[27,42], A. Jacob[13], B. Jamieson[48], R.A. Johnson[28], S. Johnson[28], J.H. Jo[2], P. Jonsson[24], C.K. Jung[2,§], M. Kabirnezhad[49], A.C. Kaboth[24], T. Kajita[46,§], H. Kakuno[50], J. Kameda[1], Y. Kanazawa[3], D. Karlen[22,43], I. Karpikov[42], T. Katori[31], E. Kearns[4,51], M. Khabibullin[42], A. Khotjantsev[42], D. Kielczewska[52], T. Kikawa[44], A. Kilinski[49], J. Kim[18], S. King[31], J. Kisiel[45], P. Kitching[53], T. Kobayashi[39,†], L. Koch[54], T. Koga[3], A. Kolaceke[11], A. Konaka[43], L.L. Kormos[38], A. Korzenev[21], Y. Koshio[55,§], W. Kropp[56], H. Kubo[44], Y. Kudenko[42,¶] R. Kurjata[36], T. Kutter[20], J. Lagoda[49], K. Laihem[54], I. Lamont[38], E. Larkin[12], M. Laveder[29], M. Lawe[26], M. Lazos[25], T. Lindner[43], C. Lister[12], R.P. Litchfield[12], A. Longhin[29], J.P. Lopez[28], L. Ludovici[57], L. Magaletti[17], K. Mahn[58], M. Malek[24], S. Manly[47], A.D. Marino[28], J. Marteau[10], J.F. Martin[33], P. Martins[31], S. Martynenko[42], T. Maruyama[39,†], V. Matveev[42], K. Mavrokoridis[25], E. Mazzucato[37], M. McCarthy[18], N. McCauley[25], K.S. McFarland[47], C. McGrew[2], A. Mefodiev[42], C. Metelko[25], M. Mezzetto[29], P. Mijakowski[49], C.A. Miller[43], A. Minamino[44], O. Mineev[42], A. Missert[28], M. Miura[1,§], S. Moriyama[1,§],

†Also at J-PARC, Tokai, Japan.
‡Also at Institute of Particle Physics, Canada.
§ Affiliated member at Kavli IPMU (WPI), University of Tokyo, Japan.
¶Also at Moscow Institute of Physics and Technology and National Research Nuclear University (MEPhI), Moscow, Russia.

Funded by SCOAP[3]

Th.A. Mueller[35], A. Murakami[44], M. Murdoch[25], S. Murphy[16], J. Myslik[22], T. Nakadaira[39,†], M. Nakahata[1,4], K.G. Nakamura[44], K. Nakamura[4,39,†], S. Nakayama[1,§], T. Nakaya[44,4], K. Nakayoshi[39,†], C. Nantais[18], C. Nielsen[18], M. Nirkko[8], K. Nishikawa[39,†], Y. Nishimura[46], J. Nowak[38], H.M. O'Keeffe[38], R. Ohta[39,†], K. Okumura[4,46], T. Okusawa[59], W. Oryszczak[52], S.M. Oser[18], T. Ovsyannikova[42], R.A. Owen[31], Y. Oyama[39,†], V. Palladino[34], J.L. Palomino[2], V. Paolone[32], D. Payne[25], O. Perevozchikov[20], J.D. Perkin[26], Y. Petrov[18], L. Pickard[26], E.S. Pinzon Guerra[19], C. Pistillo[8], P. Plonski[36], E. Poplawska[31], B. Popov[14,**], M. Posiadala-Zezula[52], J.-M. Poutissou[43], R. Poutissou[43], P. Przewlocki[49], B. Quilain[35], E. Radicioni[17], P.N. Ratoff[38], M. Ravonel[21], M.A.M. Rayner[21], A. Redij[8], M. Reeves[38], E. Reinherz-Aronis[9], C. Riccio[34], P.A. Rodrigues[47], P. Rojas[9], E. Rondio[49], S. Roth[54], A. Rubbia[16], D. Ruterbories[47], R. Sacco[31], K. Sakashita[39,†], F. Sánchez[23], F. Sato[39], E. Scantamburlo[21], K. Scholberg[5,§], S. Schoppmann[54], J. Schwehr[9], M. Scott[43], Y. Seiya[59], T. Sekiguchi[39,†], H. Sekiya[1,§], D. Sgalaberna[16], R. Shah[6,13], F. Shaker[48], M. Shiozawa[1,4], S. Short[31], Y. Shustrov[42], P. Sinclair[24], B. Smith[24], M. Smy[56], J.T. Sobczyk[41], H. Sobel[4,56], M. Sorel[27], L. Southwell[38], P. Stamoulis[27], J. Steinmann[54], B. Still[31], Y. Suda[3], A. Suzuki[7], K. Suzuki[44], S.Y. Suzuki[39,†], Y. Suzuki[4], R. Tacik[11,43], M. Tada[39,†], S. Takahashi[44], A. Takeda[1], Y. Takeuchi[4,7], H.K. Tanaka[1,§], H.A. Tanaka[18,‡], M.M. Tanaka[39,†], D. Terhorst[54], R. Terri[31], L.F. Thompson[26], A. Thorley[25], S. Tobayama[18], W. Toki[9], T. Tomura[1], Y. Totsuka[††], C. Touramanis[25], T. Tsukamoto[39,†], M. Tzanov[20], Y. Uchida[24], A. Vacheret[13], M. Vagins[4,56], G. Vasseur[37], T. Wachala[15], A.V. Waldron[13], K. Wakamatsu[59], C.W. Walter[5,§], D. Wark[6,13], W. Warzycha[52], M.O. Wascko[24], A. Weber[6,13], R. Wendell[1,§], R.J. Wilkes[30], M.J. Wilking[2], C. Wilkinson[26], Z. Williamson[13], J.R. Wilson[31], R.J. Wilson[9], T. Wongjirad[5], Y. Yamada[39,†], K. Yamamoto[59], C. Yanagisawa[2,‡‡], T. Yano[7], S. Yen[43], N. Yershov[42], M. Yokoyama[3,§], K. Yoshida[44], T. Yuan[28], M. Yu[19], A. Zalewska[15], J. Zalipska[49], L. Zambelli[39,†], K. Zaremba[36], M. Ziembicki[36], E.D. Zimmerman[28], M. Zito[37], J. Żmuda[41]

[1] *University of Tokyo, Institute for Cosmic Ray Research, Kamioka Observatory, Kamioka, Japan*
[2] *State University of New York at Stony Brook, Department of Physics and Astronomy, Stony Brook, New York, USA*
[3] *University of Tokyo, Department of Physics, Tokyo, Japan*
[4] *Kavli Institute for the Physics and Mathematics of the Universe (WPI), Todai Institutes for Advanced Study, University of Tokyo, Kashiwa, Chiba, Japan*
[5] *Duke University, Department of Physics, Durham, North Carolina, USA*
[6] *STFC, Rutherford Appleton Laboratory, Harwell Oxford, and Daresbury Laboratory, Warrington, United Kingdom*
[7] *Kobe University, Kobe, Japan*
[8] *University of Bern, Albert Einstein Center for Fundamental Physics, Laboratory for High Energy Physics (LHEP), Bern, Switzerland*
[9] *Colorado State University, Department of Physics, Fort Collins, Colorado, USA*
[10] *Université de Lyon, Université Claude Bernard Lyon 1, IPN Lyon (IN2P3), Villeurbanne, France*
[11] *University of Regina, Department of Physics, Regina, Saskatchewan, Canada*
[12] *University of Warwick, Department of Physics, Coventry, United Kingdom*
[13] *Oxford University, Department of Physics, Oxford, United Kingdom*

[**] Also at JINR, Dubna, Russia.
[††] Deceased.
[‡‡] Also at BMCC/CUNY, Science Department, New York, USA.

[14]*UPMC, Université Paris Diderot, CNRS/IN2P3, Laboratoire de Physique Nucléaire et de Hautes Energies (LPNHE), Paris, France*
[15]*H. Niewodniczanski Institute of Nuclear Physics PAN, Cracow, Poland*
[16]*ETH Zurich, Institute for Particle Physics, Zurich, Switzerland*
[17]*INFN Sezione di Bari and Università e Politecnico di Bari, Dipartimento Interuniversitario di Fisica, Bari, Italy*
[18]*University of British Columbia, Department of Physics and Astronomy, Vancouver, British Columbia, Canada*
[19]*York University, Department of Physics and Astronomy, Toronto, Ontario, Canada*
[20]*Louisiana State University, Department of Physics and Astronomy, Baton Rouge, Louisiana, USA*
[21]*University of Geneva, Section de Physique, DPNC, Geneva, Switzerland*
[22]*University of Victoria, Department of Physics and Astronomy, Victoria, British Columbia, Canada*
[23]*Institut de Fisica d'Altes Energies (IFAE), Bellaterra (Barcelona), Spain*
[24]*Imperial College London, Department of Physics, London, United Kingdom*
[25]*University of Liverpool, Department of Physics, Liverpool, United Kingdom*
[26]*University of Sheffield, Department of Physics and Astronomy, Sheffield, United Kingdom*
[27]*IFIC (CSIC & University of Valencia), Valencia, Spain*
[28]*University of Colorado at Boulder, Department of Physics, Boulder, Colorado, USA*
[29]*INFN Sezione di Padova and Università di Padova, Dipartimento di Fisica, Padova, Italy*
[30]*University of Washington, Department of Physics, Seattle, Washington, USA*
[31]*Queen Mary University of London, School of Physics and Astronomy, London, United Kingdom*
[32]*University of Pittsburgh, Department of Physics and Astronomy, Pittsburgh, Pennsylvania, USA*
[33]*University of Toronto, Department of Physics, Toronto, Ontario, Canada*
[34]*INFN Sezione di Napoli and Università di Napoli, Dipartimento di Fisica, Napoli, Italy*
[35]*Ecole Polytechnique, IN2P3-CNRS, Laboratoire Leprince-Ringuet, Palaiseau, France*
[36]*Warsaw University of Technology, Institute of Radioelectronics, Warsaw, Poland*
[37]*IRFU, CEA Saclay, Gif-sur-Yvette, France*
[38]*Lancaster University, Physics Department, Lancaster, United Kingdom*
[39]*High Energy Accelerator Research Organization (KEK), Tsukuba, Ibaraki, Japan*
[40]*Miyagi University of Education, Department of Physics, Sendai, Japan*
[41]*Wroclaw University, Faculty of Physics and Astronomy, Wroclaw, Poland*
[42]*Institute for Nuclear Research of the Russian Academy of Sciences, Moscow, Russia*
[43]*TRIUMF, Vancouver, British Columbia, Canada*
[44]*Kyoto University, Department of Physics, Kyoto, Japan*
[45]*University of Silesia, Institute of Physics, Katowice, Poland*
[46]*University of Tokyo, Institute for Cosmic Ray Research, Research Center for Cosmic Neutrinos, Kashiwa, Japan*
[47]*University of Rochester, Department of Physics and Astronomy, Rochester, New York, USA*
[48]*University of Winnipeg, Department of Physics, Winnipeg, Manitoba, Canada*
[49]*National Centre for Nuclear Research, Warsaw, Poland*
[50]*Tokyo Metropolitan University, Department of Physics, Tokyo, Japan*
[51]*Boston University, Department of Physics, Boston, Massachusetts, USA*
[52]*University of Warsaw, Faculty of Physics, Warsaw, Poland*
[53]*University of Alberta, Centre for Particle Physics, Department of Physics, Edmonton, Alberta, Canada*
[54]*RWTH Aachen University, III. Physikalisches Institut, Aachen, Germany*
[55]*Okayama University, Department of Physics, Okayama, Japan*
[56]*University of California, Irvine, Department of Physics and Astronomy, Irvine, California, USA*
[57]*INFN Sezione di Roma and Università di Roma "La Sapienza," Roma, Italy*
[58]*Michigan State University, Department of Physics and Astronomy, East Lansing, Michigan, USA*
[59]*Osaka City University, Department of Physics, Osaka, Japan*
*E-mail: ichikawa@scphys.kyoto-u.ac.jp

Received September 26, 2014; Revised January 26, 2015; Accepted January 29, 2015; Published April 1, 2015

The observation of the recent electron neutrino appearance in a muon neutrino beam and the high-precision measurement of the mixing angle θ_{13} have led to a re-evaluation of the physics potential of the T2K long-baseline neutrino oscillation experiment. Sensitivities are explored for CP violation in neutrinos, non-maximal $\sin^2 2\theta_{23}$, the octant of θ_{23}, and the mass hierarchy, in addition to the measurements of δ_{CP}, $\sin^2\theta_{23}$, and Δm^2_{32}, for various combinations of ν-mode and $\bar{\nu}$-mode data-taking.

With an exposure of 7.8×10^{21} protons-on-target, T2K can achieve $1\,\sigma$ resolution of 0.050 (0.054) on $\sin^2\theta_{23}$ and 0.040 (0.045) $\times 10^{-3}\,\mathrm{eV}^2$ on Δm^2_{32} for 100% (50%) neutrino beam mode running assuming $\sin^2\theta_{23} = 0.5$ and $\Delta m^2_{32} = 2.4 \times 10^{-3}\,\mathrm{eV}^2$. T2K will have sensitivity to the CP-violating phase δ_{CP} at 90% C.L. or better over a significant range. For example, if $\sin^2 2\theta_{23}$ is maximal (i.e. $\theta_{23} = 45^\circ$) the range is $-115^\circ < \delta_{CP} < -60^\circ$ for normal hierarchy and $+50^\circ < \delta_{CP} < +130^\circ$ for inverted hierarchy. When T2K data is combined with data from the NOνA experiment, the region of oscillation parameter space where there is sensitivity to observe a non-zero δ_{CP} is substantially increased compared to if each experiment is analyzed alone.

1. Introduction

The experimental confirmation of neutrino oscillations, where neutrinos of a particular flavor (ν_e, ν_μ, ν_τ) can transmute to another flavor, has profound implications for physics. The observation of a zenith-angle-dependent deficit in muon neutrinos produced by high-energy proton interactions in the atmosphere [1] confirmed the neutrino flavor oscillation hypothesis. The "anomalous" solar neutrino flux [2] problem was shown to be due to neutrino oscillation by more precise measurements [3–6]. Atmospheric neutrino measurements have provided further precision on the disappearance of muon neutrinos [7,8] and the appearance of tau neutrinos [9]. Taking advantage of nuclear reactors as intense sources, the disappearance of electron antineutrinos has been firmly established using both widely distributed multiple sources at an average distance of 180 km [6] and from specialized detectors placed within ∼2 km [10–12]. The development of high-intensity proton accelerators that can produce focused neutrino beams with mean energy from a few hundred MeV to tens of GeV have enabled measurements of the disappearance of muon neutrinos (and muon antineutrinos) [8,13,14] and appearance of electron neutrinos (and electron antineutrinos) [15–18] and tau neutrinos [19] over distances of hundreds of kilometers.

While the early solar and atmospheric oscillation experiments could be described in a two-neutrino framework, recent experiments with diverse neutrino sources support a three-flavor oscillation framework. In this scenario, the three neutrino flavor eigenstates mix with three mass eigenstates (ν_1, ν_2, ν_3) through the Pontecorvo–Maki–Nakagawa–Sakata [20] (PMNS) matrix in terms of three mixing angles (θ_{12}, θ_{23}, θ_{13}) and one complex phase (δ_{CP}). The probability of neutrino oscillation depends on these parameters, as well as the difference of the squared masses of the mass states $\left(\Delta m^2_{21}, \Delta m^2_{31}, \Delta m^2_{32}\right)$. Furthermore, there is an explicit dependence on the energy of the neutrino (E_ν) and the distance traveled (L) before detection. To date, all the experimental results are well described within the neutrino oscillation framework as described in Sect. 2.

T2K is a long-baseline neutrino oscillation experiment proposed in 2003 [21] with three main physics goals that were to be achieved with data corresponding to 7.8×10^{21} protons-on-target (POT) from a 30 GeV proton beam:

- search for $\nu_\mu \to \nu_e$ appearance and establish that $\theta_{13} \neq 0$ with a sensitivity down to $\sin^2 2\theta_{13} \sim 0.008$ (90% C.L.);

- precision measurement of oscillation parameters in ν_μ disappearance with $\delta\left(\Delta m^2_{32}\right) \sim 10^{-4}\,\mathrm{eV}^2$ and $\delta\left(\sin^2 2\theta_{23}\right) \sim 0.01$; and
- search for sterile components in ν_μ disappearance.

The T2K experiment began data-taking in 2009 [22] and a major physics goal, the discovery of $\nu_\mu \to \nu_e$ appearance, has been realized at a $7.3\,\sigma$ level of significance with just 8.4% of the total approved POT [17]. This is the first time an explicit flavor appearance has been observed from another neutrino flavor with significance larger than $5\,\sigma$. This observation opens the door to study CP violation (CPV) in neutrinos, as described in Sect. 2. Following this discovery, the primary physics goal for the neutrino physics community has become a detailed investigation of the three-flavor paradigm, which requires determination of the CP-violating phase δ_{CP}, resolution of the mass hierarchy (MH), precise measurement of θ_{23} to determine how close θ_{23} is to 45°, and determination of the θ_{23} octant, i.e., whether the mixing angle θ_{23} is less than or greater than 45°. T2K, along with the NOνA [23] experiment that recently began operation, will lead in the determination of these parameters for at least a decade.

This paper provides a comprehensive update of the anticipated sensitivity of the T2K experiment to the oscillation parameters as given in the original T2K proposal [21], and includes an investigation of the enhancements from performing combined fits including the projected NOνA sensitivity. It starts with a brief overview of the neutrino oscillation framework in Sect. 2, and a description of the T2K experiment in Sect. 3. Updated T2K sensitivities are given in Sect. 4, while sensitivities when results from T2K are combined with those from the NOνA experiment are given in Sect. 5. Finally, results of a study of the optimization of the ν and $\bar{\nu}$ running time for both T2K and NOνA are given in Sect. 6.

2. Neutrino mixing and oscillation framework

Three-generation neutrino mixing can be described by a unitary matrix, often referred to as the PMNS matrix. The weak flavor eigenstates ν_e, ν_μ, and ν_τ are related to the mass eigenstates, ν_1, ν_2, and ν_3, by the unitary mixing matrix U:

$$\begin{pmatrix} \nu_e \\ \nu_\mu \\ \nu_\tau \end{pmatrix} = \begin{bmatrix} U_{e1} & U_{e2} & U_{e3} \\ U_{\mu 1} & U_{\mu 2} & U_{\mu 3} \\ U_{\tau 1} & U_{\tau 2} & U_{\tau 3} \end{bmatrix} \begin{pmatrix} \nu_1 \\ \nu_2 \\ \nu_3 \end{pmatrix}, \tag{1}$$

where the matrix is commonly parameterized as

$$U_{\mathrm{PMNS}} = \begin{bmatrix} 1 & 0 & 0 \\ 0 & C_{23} & S_{23} \\ 0 & -S_{23} & C_{23} \end{bmatrix} \begin{bmatrix} C_{13} & 0 & S_{13}e^{-i\delta_{\mathrm{CP}}} \\ 0 & 1 & 0 \\ -S_{13}e^{+i\delta_{\mathrm{CP}}} & 0 & C_{13} \end{bmatrix} \begin{bmatrix} C_{12} & S_{12} & 0 \\ -S_{12} & C_{12} & 0 \\ 0 & 0 & 1 \end{bmatrix}, \tag{2}$$

with C_{ij} $\left(S_{ij}\right)$ representing $\cos\theta_{ij}$ $\left(\sin\theta_{ij}\right)$, where θ_{ij} is the mixing angle between the generations i and j. There is one irreducible phase, δ_{CP}, allowed in a unitary 3×3 mixing matrix.[1] After neutrinos propagate through vacuum, the probability that they will interact via one of the three flavors will depend on the values of these mixing angles. As neutrinos propagate through matter, coherent forward scattering of electron neutrinos causes a change in the effective neutrino mass that leads to

[1] If the neutrino is a Majorana particle, two additional phases are allowed that have no consequences for neutrino oscillations.

a modification of the oscillation probability. This is the so-called *matter effect*. Interference between multiple terms in the transition probability can lead to CP violation in neutrino mixing if the phase $\delta_{\rm CP}$ is non-zero.

For T2K, the neutrino oscillation modes of interest are the $\nu_\mu \to \nu_e$ appearance mode and the ν_μ disappearance mode. The $\nu_\mu \to \nu_e$ appearance oscillation probability (to first order approximation in the matter effect [24]) is given by

$$\begin{aligned} P(\nu_\mu \to \nu_e) = {} & 4C_{13}^2 S_{13}^2 S_{23}^2 \sin^2\Phi_{31} \left(1 + \frac{2a}{\Delta m_{31}^2}\left(1 - 2S_{13}^2\right)\right) \\ & + 8C_{13}^2 S_{12} S_{13} S_{23} \left(C_{12} C_{23} \cos\delta_{\rm CP} - S_{12} S_{13} S_{23}\right) \cos\Phi_{32} \sin\Phi_{31} \sin\Phi_{21} \\ & - 8C_{13}^2 C_{12} C_{23} S_{12} S_{13} S_{23} \sin\delta_{\rm CP} \sin\Phi_{32} \sin\Phi_{31} \sin\Phi_{21} \\ & + 4S_{12}^2 C_{13}^2 \left(C_{12}^2 C_{23}^2 + S_{12}^2 S_{23}^2 S_{13}^2 - 2C_{12} C_{23} S_{12} S_{23} S_{13} \cos\delta_{\rm CP}\right) \sin^2\Phi_{21} \\ & - 8C_{13}^2 S_{13}^2 S_{23}^2 \left(1 - 2S_{13}^2\right) \frac{aL}{4E_\nu} \cos\Phi_{32} \sin\Phi_{31}, \end{aligned} \tag{3}$$

where $\Phi_{ji} = \Delta m_{ji}^2 L/4E_\nu$. The terms that include

$$a \equiv 2\sqrt{2} G_{\rm F} n_e E_\nu = 7.56 \times 10^{-5} \left[{\rm eV}^2\right] \left(\frac{\rho}{[{\rm g\,cm}^{-3}]}\right) \left(\frac{E_\nu}{[{\rm GeV}]}\right)$$

are a consequence of the matter effect, where n_e and ρ are the electron and matter densities, respectively. The equivalent expression for antineutrino appearance, $\bar{\nu}_\mu \to \bar{\nu}_e$, is obtained by reversing the signs of terms proportional to $\sin\delta_{\rm CP}$ and a. The first and fourth terms of Eq. (3) come from oscillations induced by θ_{13} and θ_{12}, respectively, in the presence of non-zero θ_{23}. The second and third terms come from interference caused by these oscillations. At the T2K peak energy of $\sim$0.6 GeV and baseline length of $L = 295$ km, $\cos\Phi_{32}$ is nearly zero and the second and fifth terms vanish. The fourth term, to which solar neutrino disappearance is attributed, is negligibly small. Hence, the dominant contribution for ν_e appearance in the T2K experiment comes from the first and third terms. The contribution from the matter effect is about 10% of the first term without the matter effect. Since the third term contains $\sin\delta_{\rm CP}$, it is called the "CP-violating" term. It is as large as 27% of the first term without the matter effect when $\sin\delta_{\rm CP} = 1$ and $\sin^2 2\theta_{23} = 1$, meaning that the CP-violating term makes a non-negligible contribution to the total ν_e appearance probability. The measurement of θ_{13} from the reactor experiments is independent of the CP phase, and future measurements from Daya Bay [10], Double Chooz [11], and RENO [12] will reduce the θ_{13} uncertainty such that the significance of the CP-violating term will be enhanced for T2K. It is also important to recognize that since the sign of the CP-violating term is opposite for neutrino and antineutrino oscillations, data taken by T2K with an antineutrino beam for comparison to neutrino data may allow us to study CP violation effects directly.

The ν_μ disappearance oscillation probability is given by

$$1 - P\left(\nu_\mu \to \nu_\mu\right) = \left(C_{13}^4 \sin^2 2\theta_{23} + S_{23}^2 \sin^2 2\theta_{13}\right) \sin^2\Phi_{32} \tag{4}$$

(where other matter effects and Δm_{21}^2 terms can be neglected). The ν_μ disappearance measurement is sensitive to $\sin^2 2\theta_{23}$ and Δm_{32}^2. Currently, the measured value of $\sin^2 2\theta_{23}$ is consistent with full mixing, but more data are required to know if that is the case. If the mixing is not maximal, the ν_e appearance data, together with the ν_μ disappearance data, have the potential to resolve the θ_{23} octant degeneracy because the first term of Eq. (3) is proportional to $\sin^2\theta_{23}$.

Table 1. Neutrino oscillation parameters from [25].

Parameter	Value
$\sin^2 2\theta_{12}$	0.857 ± 0.024
$\sin^2 2\theta_{23}$	>0.95
$\sin^2 2\theta_{13}$	0.095 ± 0.010
Δm^2_{21}	$(7.5 \pm 0.20) \times 10^{-5}\,\mathrm{eV}^2$
$\lvert\Delta m^2_{32}\rvert$	$(2.32^{+0.12}_{-0.08}) \times 10^{-3}\,\mathrm{eV}^2$
δ_{CP}	unknown

The NOνA experiment is similar to T2K in the basic goals to measure ν_μ disappearance and ν_e appearance in an off-axis muon neutrino beam. The most important difference between the two experiments is the distance from the neutrino source to the far detector, 810 km for NOνA and 295 km for T2K, with a correspondingly higher peak neutrino beam energy for NOνA to maximize the appearance probability. NOνA is projected to have similar sensitivity compared to T2K for θ_{23}, θ_{13}, and δ_{CP}, but better sensitivity to the sign of Δm^2_{32} since, as can be seen in a in Eq. (3), the size of the matter effect is proportional to the distance L. The combination of results from the two experiments at different baselines will further improve the sensitivity to the sign of Δm^2_{32} and to δ_{CP}.

In this paper we present the updated T2K sensitivity to neutrino oscillation parameters using a large value of $\sin^2 2\theta_{13}$ similar to that measured by the reactor experiments, together with the sensitivity when projected T2K and NOνA results are combined.

The latest measured values of the neutrino mixing parameters $\left(\theta_{12}, \theta_{23}, \theta_{13}, \lvert\Delta m^2_{32}\rvert, \Delta m^2_{21}, \delta_{\mathrm{CP}}\right)$ are listed in Table 1 [25]. The CP-violating phase, δ_{CP}, is not yet well constrained, nor is the sign of $\Delta m^2_{32} \equiv m^2_3 - m^2_2$ known. The sign of Δm^2_{32} is related to the ordering of the three mass eigenstates; the positive sign is referred to as the normal MH (NH) and the negative sign as the inverted MH (IH). Of the mixing angles, the angle θ_{23} is measured with the least precision; the value of $\sin^2 2\theta_{23}$ in Table 1 corresponds to $0.4 < \sin^2(\theta_{23}) < 0.6$. Many theoretical models, e.g. some based on flavor symmetries and some on random draws on parameter spaces, sometimes try to explain the origin of the PMNS matrix together with the Cabibbo–Kobayashi–Maskawa matrix, which describes mixing in the quark sector. Precise determination of how close this mixing angle is to 45° would be an important element in understanding the origin of flavor mixing of both quarks and leptons.

3. T2K experiment

The T2K experiment [22] uses a 30 GeV proton beam accelerated by the J-PARC accelerator facility. This is composed of (1) the muon neutrino beamline; (2) the near detector complex, which is located 280 m downstream of the neutrino production target, monitors the beam, and constrains the neutrino flux parameterization and cross sections; and (3) the far detector, Super-Kamiokande (Super-K), which detects neutrinos at a baseline distance of 295 km from the target. The neutrino beam is directed 2.5° away from Super-K, producing a narrow-band ν_μ beam [26] at the far detector. The off-axis angle is chosen such that the energy peaks at $E_\nu = \Delta m^2_{32} L/2\pi \approx 0.6$ GeV, which corresponds to the first oscillation minimum of the ν_μ survival probability at Super-K. This enhances the sensitivity to θ_{13} and θ_{23} and reduces backgrounds from higher-energy neutrino interactions at Super-K.

The J-PARC main ring accelerator provides a fast-extracted high-intensity proton beam to a graphite target located in the first of three consecutive electromagnetic horns. Pions and kaons produced in the target are focused by the horns and decay in flight to muons and ν_μs in the helium-filled

96 m-long decay tunnel. This is followed by a beam dump and a set of muon monitors, which are used to monitor the direction and stability of the neutrino beam.

The near detector complex contains an on-axis Interactive Neutrino Grid detector (INGRID) [27] and an off-axis magnetized detector, ND280. INGRID measures the neutrino interaction event rate at various positions from 0° to $\sim 1^\circ$ around the beam axis, and provides monitoring of the intensity, direction, profile, and stability of the neutrino beam. The ND280 off-axis detector measures neutrino beam properties and neutrino interactions at approximately the same off-axis angle as Super-K. It is enclosed in a 0.2 T magnet that contains a subdetector optimized to measure π^0s (PØD) [28], three time projection chambers (TPC1,2,3) [29] alternating with two one-tonne fine-grained detectors (FGD1,2) [30], and an electromagnetic calorimeter (ECal) that surrounds the TPC, FGD, and PØD detectors. A side muon range detector (SMRD) [31] built into slots in the magnet return-yoke steel detects muons that exit or stop in the magnet steel. A schematic diagram of the detector layout has been published elsewhere [22].

The Super-K water Cherenkov far detector [32] has a fiducial mass of 22.5 kt contained within a cylindrical inner detector (ID) instrumented with 11,129 inward facing 20 in phototubes. Surrounding the ID is a 2 m-wide outer detector (OD) with 1,885 outward-facing 8 in phototubes. A Global Positioning System receiver with <150 ns precision synchronizes the timing between reconstructed Super-K events and the J-PARC beam spill.

T2K employs various analysis methods to estimate oscillation parameters from the data, but in general it is done by comparing the observed and predicted ν_e and ν_μ interaction rates and energy spectra at the far detector. The rate and spectrum depend on the oscillation parameters, the incident neutrino flux, neutrino interaction cross sections, and the detector response. The initial estimate of the neutrino flux is determined from detailed simulations incorporating proton beam measurements, INGRID measurements, and pion and kaon production measurements from the NA61/SHINE [33,34] experiment. The ND280 detector measurement of ν_μ charged current (CC) events is used to constrain the initial flux estimates and parameters of the neutrino interaction models that affect the predicted rate and spectrum of neutrino interactions at both ND280 and Super-K. At Super-K, ν_e and ν_μ charged current quasi-elastic (CCQE) events, for which the neutrino energy can be reconstructed using simple kinematics, are selected. Efficiencies and backgrounds are determined through detailed simulations tuned to control samples which account for final state interactions (FSI) inside the nucleus and secondary hadronic interactions (SI) in the detector material. These combined results are used in a fit to determine the oscillation parameters.

As of May 2013, T2K has accumulated 6.57×10^{20} POT, which corresponds to about 8.4% of the total approved data. Results from this dataset on the measurement of θ_{23} and $|\Delta m^2_{32}|$ by ν_μ disappearance [14], and of θ_{13} and $\delta_{\rm CP}$ by ν_e appearance, have been published [17]. It is reported in [17] that combining the T2K result with the world average value of θ_{13} from reactor experiments leads to some values of $\delta_{\rm CP}$ being disfavored at 90% CL.

4. T2K projected sensitivities to neutrino oscillation parameters

To demonstrate the T2K physics potential, we have performed sensitivity studies using combined fits to the reconstructed energy spectra of $\nu_e(\bar{\nu}_e)$ and $\nu_\mu(\bar{\nu}_\mu)$ events observed at Super-K with both ν-mode and $\bar{\nu}$-mode beams in the three-flavor mixing model. The results shown here generally use the systematic errors established for the 2012 oscillation analyses [16,35] as described below, although, in addition, we have studied cases with projected systematic errors as described in Sect. 4.5.

Since the sensitivity depends on the true values of the oscillation parameters, a set of oscillation parameters (θ) is chosen as a test point for each study and is used to generate simulated "observed" reconstructed energy spectra. Then, a hypothesis test for the set of parameters of interest (H_0) is applied using

$$\Delta\chi^2 = \chi^2(H_0) - \chi^2_{\rm min}. \tag{5}$$

The value of $\chi^2(H_0)$ is calculated as $-2\ln\mathcal{L}(\theta|H_0)$, where $\mathcal{L}(\theta|H_0)$ is the likelihood to observe the spectrum generated at θ when the "true" oscillation parameters are given by H_0. The minimum value of χ^2 in the oscillation parameter space is given by $\chi^2_{\rm min}$. The oscillation parameter set which gives $\chi^2_{\rm min}$ is equivalent to θ, since spectra are generated without statistical fluctuations in this analysis. When we test only one or two of the five varied oscillation parameters ($\sin^2 2\theta_{13}$, $\delta_{\rm CP}$, $\sin^2\theta_{23}$, Δm^2_{32}, and the MH), the tested parameters are fixed at a set of test points, and the remaining oscillation parameters are fitted to give a minimized $\chi^2(H_0)$.

In most cases, this $\Delta\chi^2$ closely resembles a χ^2 distribution for n degrees of freedom, where n corresponds to the number of tested oscillation parameters. Then, critical χ^2 values for Gaussian distributed variables ($\Delta\chi^2_{\rm critical}$) can be used for determining confidence level (C.L.) regions [36]. Each simulated spectrum is generated at the MC sample statistical mean, and therefore the results of this test represent the median sensitivity. Thus the results of these studies indicate that half of experiments are expected to be able to reject H_0 at the reported C.L. This is accurate if two conditions are met: (1) the probability density function (pdf) for $\Delta\chi^2$ follows a true χ^2 distribution, and (2) the $\Delta\chi^2$ value calculated with the MC sample statistical mean spectra ($\bar{\Delta}\chi^2$) is equivalent to the median of the $\Delta\chi^2$ pdf. Then, $\bar{\Delta}\chi^2$ can be used to construct median sensitivity C.L. contours. Studies using ensembles of toy MC experiments where statistical fluctuations expected at a given POT and systematic fluctuations are included have shown that calculating C.L.s by applying a $\Delta\chi^2_{\rm critical}$ value to $\Delta\chi^2$ gives fairly consistent C.L.s, and that $\bar{\Delta}\chi^2$ is in good agreement with the median $\Delta\chi^2$ value of each ensemble of toy MC experiments, except in the case of a mass hierarchy determination. Therefore, in this paper we show C.L.s constructed by applying the $\Delta\chi^2_{\rm critical}$ value to $\Delta\bar{\chi}^2$ as our median sensitivity. The exception of the MH case will be discussed in detail in Sect. 5.

4.1. Expected observables and summary of current systematic errors

Our sensitivity studies are based on the signal efficiency, background, and systematic errors established for the T2K 2012 oscillation analyses [16,35]; however, we note that errors are lower in more recent published analyses. Since official T2K systematic errors are used, these errors have been reliably estimated based on data analysis, unlike previous sensitivity studies which used errors based only on simulation and estimations [21]. Systematic errors therefore include both normalization and shape errors, and are implemented as a covariance matrix for these studies, where full correlation between ν- and $\bar{\nu}$-modes is generally assumed.

For the ν_e sample, interaction candidate events fully contained in the fiducial volume with a single electron-like Cherenkov ring are selected. The visible energy is required to exceed 100 MeV/c, events with a delayed electron signal are rejected, and events with an invariant mass near that of the π^0 are rejected, where the invariant mass is reconstructed assuming the existence of a second ring. Finally, events are required to have a reconstructed neutrino energy below 1250 MeV. The efficiency of the event selection for the CC ν_e signal is 62% and the fraction of CCQE events in the signal is 80%. For the ν_μ sample, again events must be fully contained in the fiducial volume, but they must now have a single muon-like Cherenkov ring with a momentum exceeding 200 MeV/c. There must be either

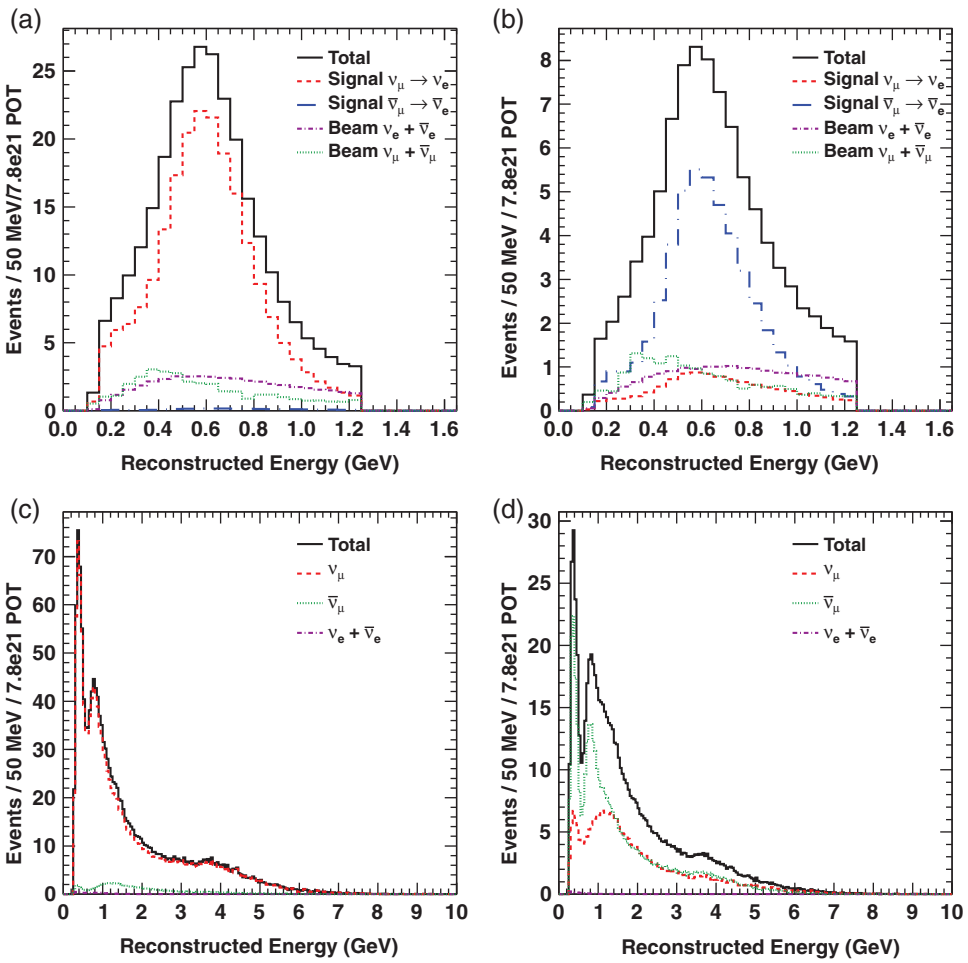

Fig. 1. Appearance and disappearance reconstructed energy spectra in Super-K for ν_e, ν_μ, $\bar{\nu}_e$, and $\bar{\nu}_\mu$ at 7.8×10^{21} POT for the nominal oscillation parameters as given in Table 2. (a) ν_e appearance reconstructed energy spectrum,100% ν-mode running, (b) $\bar{\nu}_e$ appearance reconstructed energy spectrum, 100% $\bar{\nu}$-mode running. (c) ν_μ disappearance reconstructed energy spectrum, 100% ν-mode running. (d) $\bar{\nu}_\mu$ disappearance reconstructed energy spectrum, 100% $\bar{\nu}$-mode running.

zero or one delayed electron. The efficiency and purity of ν_μ CCQE events are estimated to be 72% and 61%, respectively.

Fits are performed by calculating $\Delta\chi^2$ using a binned likelihood method for the appearance and disappearance reconstructed energy spectra in Super-K. Reconstructed appearance and disappearance energy spectra generated for the approved full T2K statistics, 7.8×10^{21} POT, assuming a data-taking condition of either 100% ν-mode or 100% $\bar{\nu}$-mode, are given in Fig. 1. These spectra are generated assuming the nominal oscillation parameters given in Table 2.

Although errors on the shape of the reconstructed energy spectra are used for the analysis described in Sect. 4, the total error on the number of events at Super-K is given in Table 3. This includes uncertainties on the flux prediction, uncertainties on ν interactions both constrained by the near detector and measured by external experiments, Super-K detector errors, and FSI uncertainties, all of which can cause fluctuations in the shape of the final reconstructed energy spectra.

When performing fits, the oscillation parameters δ_{CP}, $\sin^2 2\theta_{13}$, $\sin^2 \theta_{23}$, and Δm^2_{32} are considered unknown unless otherwise stated, while $\sin^2 2\theta_{12}$ and Δm^2_{21} are assumed fixed to the values given in this table. Tables 4 and 5 give the number of events expected with the T2K full statistics. Figure 2

Table 2. Nominal values of the oscillation parameters. When the reactor constraint is used, we assume 0.005 as the expected uncertainty of the reactor measurement.

Parameter	$\sin^2 2\theta_{13}$	δ_{CP}	$\sin^2 \theta_{23}$	Δm^2_{32}	Hierarchy	$\sin^2 2\theta_{12}$	Δm^2_{21}
Nominal Value	0.1	0	0.5	2.4×10^{-3} eV^2	normal	0.8704	7.6×10^{-5} eV^2

Table 3. The systematic errors in percentage on the predicted number of events at Super-K (assuming the oscillation parameters given in Table 2 are the true values of the oscillation parameters) as used in the 2012 oscillation analyses.

	Appearance	Disappearance
Flux and cross section constrained by the near detector	5.0%	4.2%
Cross section not constrained by the near detector	7.4%	6.2%
Super-K detector and FSI	3.9%	11.0%
Total	9.7%	13.3%

Table 4. Expected numbers of ν_e or $\bar{\nu}_e$ appearance events at 7.8×10^{21} POT. The number of events is broken down into those coming from: appearance signal or intrinsic beam background events that undergo charged current (CC) interactions in Super-K, or beam background events that undergo neutral current (NC) interactions.

	δ_{CP}	Total	Signal $\nu_\mu \to \nu_e$	Signal $\bar{\nu}_\mu \to \bar{\nu}_e$	Beam CC $\nu_e + \bar{\nu}_e$	Beam CC $\nu_\mu + \bar{\nu}_\mu$	NC
100% ν-mode	0°	291.5	211.9	2.4	41.3	1.4	34.5
100% ν-mode	-90°	341.8	262.9	1.7			
100% $\bar{\nu}$-mode	0°	94.9	11.2	48.8	17.2	0.4	17.3
100% $\bar{\nu}$-mode	-90°	82.9	13.1	34.9			

Table 5. Expected numbers of ν_μ or $\bar{\nu}_\mu$ disappearance events for 7.8×10^{21} POT. The first two columns show the number of ν_μ and $\bar{\nu}_\mu$ events, broken down into those that undergo charged-current quasi-elastic (CCQE) scattering at Super-K, and those that undergo other types of CC scattering (CC non-QE). The third column shows CC ν_e and $\bar{\nu}$ events, both from intrinsic beam backgrounds and oscillations, while the fourth column shows NC events.

	Total	CCQE $\nu_\mu(\bar{\nu}_\mu)$	CC non-QE $\nu_\mu(\bar{\nu}_\mu)$	CC $\nu_e + \bar{\nu}_e$ CC $\nu_\mu(\bar{\nu}_\mu) \to \nu_e(\bar{\nu}_e)$	NC
100% running in ν-mode	1,493	782 (48)	544 (40)	4	75
100% running in $\bar{\nu}$-mode	715	130 (263)	151 (138)	0.5	33

shows the dependence of the ν_e appearance reconstructed energy spectrum on δ_{CP}. Some of the sensitivities are enhanced by constraining the error on $\sin^2 2\theta_{13}$ based on the projected precision of reactor measurements. For this study, the uncertainty (referred to as the ultimate reactor error) on $\sin^2 2\theta_{13}$ is chosen to be 0.005, which corresponds to the 2012 systematic error only of the Daya Bay experiment [37].[2]

[2] The statistical error is 0.010 for [37].

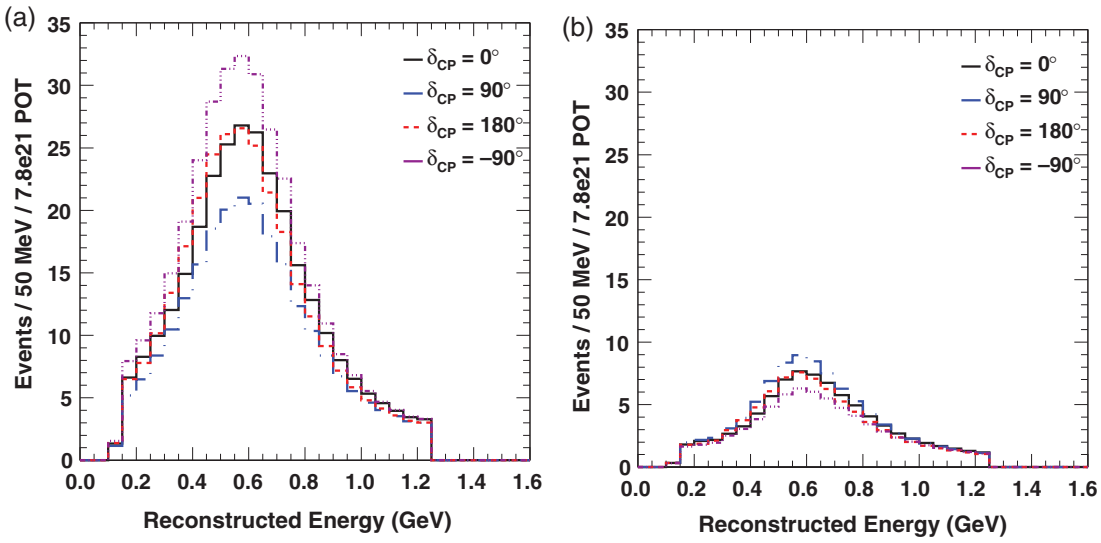

Fig. 2. ν_e appearance reconstructed energy spectra in Super-K for 7.8×10^{21} POT in either ν-mode or $\bar{\nu}$-mode at various values of assumed true δ_{CP} with $\sin^2\theta_{23} = 0.5$. (a) ν-mode running, (b) $\bar{\nu}$-mode running.

4.2. Expected 90% C.L. regions

In this section we show expected 90% C.L. intervals for the T2K full statistics of 7.8×10^{21} POT. Contours showing both the T2K sensitivity for δ_{CP} vs. $\sin^2 2\theta_{13}$ and for Δm^2_{32} vs. $\sin^2\theta_{23}$ are provided, where the assumed true value of the oscillation parameters is indicated by a black cross. The oscillation parameters δ_{CP}, $\sin^2 2\theta_{13}$, $\sin^2\theta_{23}$, and Δm^2_{32} are considered unknown, as stated above. Both the NH and IH are considered, and $\Delta\chi^2$ values are calculated from the minimum χ^2 value for both MH assumptions. The blue curves are generated assuming the correct MH and the red curves are generated assuming the incorrect MH, such that if an experiment or combination of experiments from the global neutrino community were to determine the MH the red contour would be eliminated. A contour consisting of the outermost edge of all contours in each plot can be considered as the T2K sensitivity assuming an unknown MH. For the sake of brevity, only results assuming true NH are shown; similar conclusions can be drawn from plots assuming true IH.

Figure 3 gives an example of the difference in the shape of the T2K sensitive region for ν- vs. $\bar{\nu}$-mode at true $\delta_{CP} = -90°$ (and the other oscillation parameters as given in Table 2) by comparing the ν-mode [Fig. 3(a)] and $\bar{\nu}$-mode [Fig. 3(b)] C.L. contours without a reactor constraint at 50% of the full T2K POT. These two contours are then combined in Fig. 3(c), which shows the 90% C.L. region for 50% ν- plus 50% $\bar{\nu}$-mode running to achieve the full T2K POT. This demonstrates that δ_{CP} can be constrained by combining ν-mode and $\bar{\nu}$-mode data.

Figures 4 and 5 show example 90% C.L. regions for δ_{CP} vs. $\sin^2 2\theta_{13}$ at the full T2K statistics, both for T2K alone and including an extra constraint on the T2K predicted data fit based on the ultimate reactor error $\delta(\sin^2 2\theta_{13}) = 0.005$ as discussed above, for true δ_{CP} of 0° and −90°, respectively. In the case of $\delta_{CP} = -90°$, we start to have sensitivity to resolve δ_{CP} without degeneracies.

Figure 6 shows example 90% C.L. regions for Δm^2_{32} vs. $\sin^2\theta_{23}$ at the full T2K statistics for $\sin^2\theta_{23} = 0.4$. The θ_{23} octant can be resolved in this case by combining both ν-mode and $\bar{\nu}$-mode data and also including a reactor constraint on θ_{13}, where this combination of inputs is required to resolve degeneracies between the oscillation parameters $\sin^2\theta_{23}$, $\sin^2 2\theta_{13}$, and δ_{CP}, demonstrating the importance of the reactor constraint in this case.

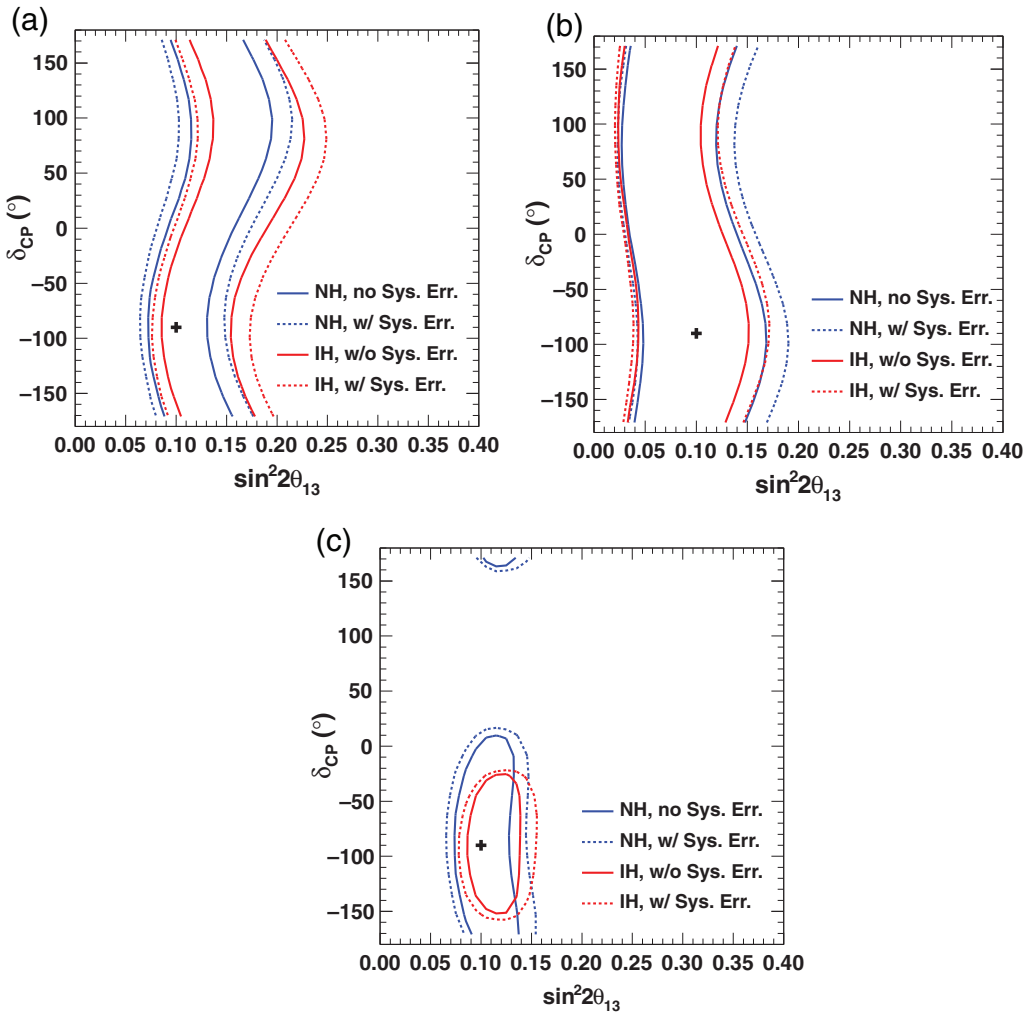

Fig. 3. Expected δ_{CP} vs. $\sin^2 2\theta_{13}$ 90% C.L. intervals, where (a) and (b) are each given for 50% of the full T2K POT, and (c) demonstrates the sensitivity of the total T2K POT with 50% ν-mode plus 50% $\bar{\nu}$-mode running. Contours are plotted for the case of true $\delta_{CP} = -90^\circ$ and NH. The blue curves are fitted assuming the correct MH(NH), while the red are fitted assuming the incorrect MH(IH), and contours are plotted from the minimum χ^2 value for both MH assumptions. The solid contours are with statistical error only, while the dashed contours include the systematic errors used in the 2012 oscillation analysis assuming full correlation between ν- and $\bar{\nu}$-mode running errors. (a) 50% ν-mode only. (b) 50% $\bar{\nu}$-mode only. (c) 50% ν, 50% $\bar{\nu}$-mode.

4.3. Sensitivities for CP-violating term, non-maximal θ_{23}, and θ_{23} octant

The sensitivities for CP violation, non-maximal θ_{23}, and the octant of θ_{23} (i.e., whether the mixing angle θ_{23} is less than or greater than 45°) depend on the true oscillation parameter values. Figure 7 shows the expected $\Delta\chi^2$ for the $\sin\delta_{CP} = 0$ hypothesis, for various true values of δ_{CP} and $\sin^2\theta_{23}$. To see the dependence more clearly, $\Delta\chi^2$ is plotted as a function of δ_{CP} for various values of $\sin^2\theta_{23}$ in Fig. 8 (normal MH case) and Fig. 9 (inverted MH case). For favorable sets of the oscillation parameters and mass hierarchy, T2K will have greater than 90% C.L. sensitivity to non-zero $\sin\delta_{CP}$.

Figures 10 and 11 show the $\sin^2\theta_{23}$ vs. δ_{CP} regions where T2K has more than a 90% C.L. sensitivity to reject maximal mixing or reject one octant of θ_{23}. In each of these figures, the oscillation parameters δ_{CP}, $\sin^2 2\theta_{13}$, $\sin^2\theta_{23}$, Δm^2_{32}, and the MH are considered unknown and a constraint based on the ultimate reactor error is used. Note that the T2K sensitivity to reject maximal mixing

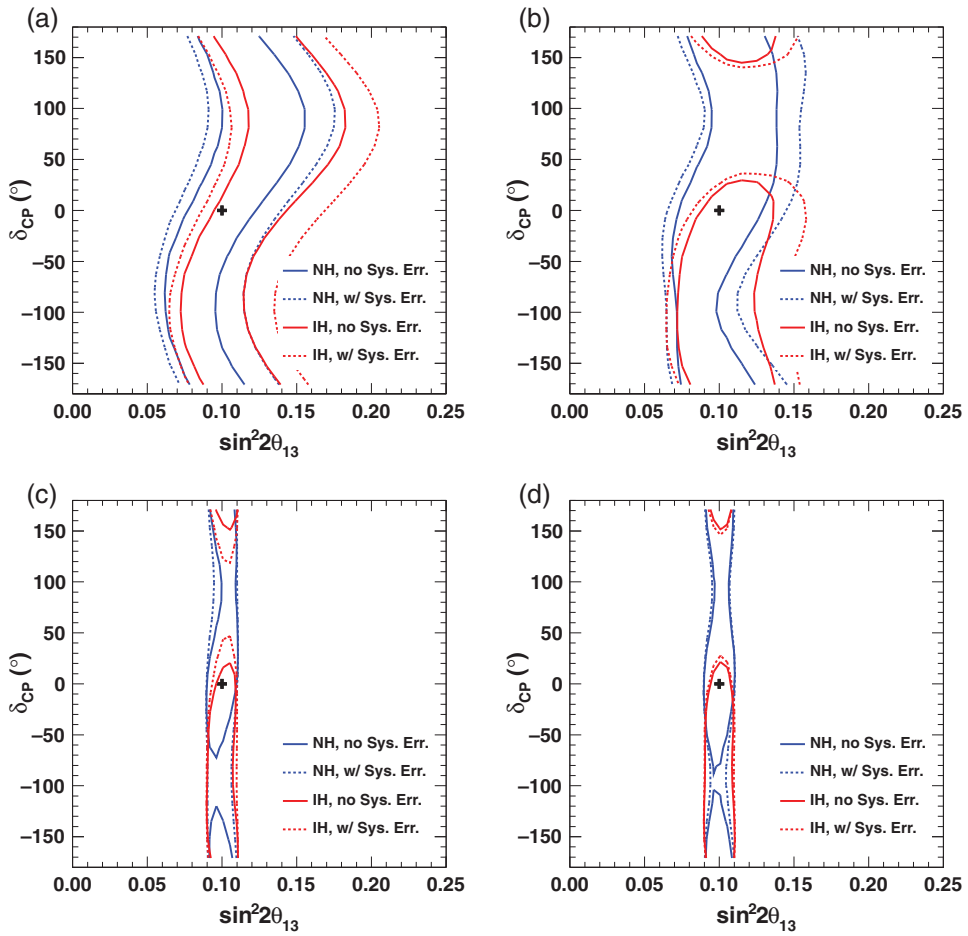

Fig. 4. δ_{CP} vs. $\sin^2 2\theta_{13}$ 90% C.L. intervals for 7.8×10^{21} POT. Contours are plotted for the case of true $\delta_{CP} = 0^\circ$ and NH. The blue curves are fitted assuming the correct MH(NH), while the red are fitted assuming the incorrect MH(IH), and contours are plotted from the minimum χ^2 value for both MH assumptions. The solid contours are with statistical error only, while the dashed contours include the 2012 systematic errors fully correlated between ν- and $\bar{\nu}$-mode. (a) 100% ν-mode. (b) 50% ν-, 50% $\bar{\nu}$-mode. (c) 100% ν-mode, with ultimate reactor constraint. (d) 50% ν-, 50% $\bar{\nu}$-mode, with ultimate reactor constraint.

is roughly independent of ν–$\bar{\nu}$ running ratio, while the sensitivity to reject one octant is better when ν- and $\bar{\nu}$-modes are combined. Again, the combination of ν- and $\bar{\nu}$-modes, as well as the tight constraint on θ_{13} from the reactor measurement, are all required to resolve the correct values for the parameters $\sin^2\theta_{23}$, $\sin^2 2\theta_{13}$, and δ_{CP} from many possible solutions. Resolving the values of these three oscillation parameters is required in order to also resolve the θ_{23} octant.

These figures show that by running with a significant amount of $\bar{\nu}$-mode, T2K has sensitivity to the CP-violating term and octant of θ_{23} for a wider region of oscillation parameters (δ_{CP}, θ_{23}) and for both mass hierarchies, particularly when systematic errors are taken into account. The optimal running ratio is discussed in more detail in Sect. 6.

4.4. Precision or sensitivity vs. POT

The T2K uncertainty (i.e. precision) vs. POT for $\sin^2\theta_{23}$ and Δm^2_{32} is given in Fig. 12 for the 100% ν-mode running case and the 50% plus 50% $\nu - \bar{\nu}$-mode running case. The precision includes either statistical errors only, statistical errors combined with the 2012 systematic errors, or statistical errors

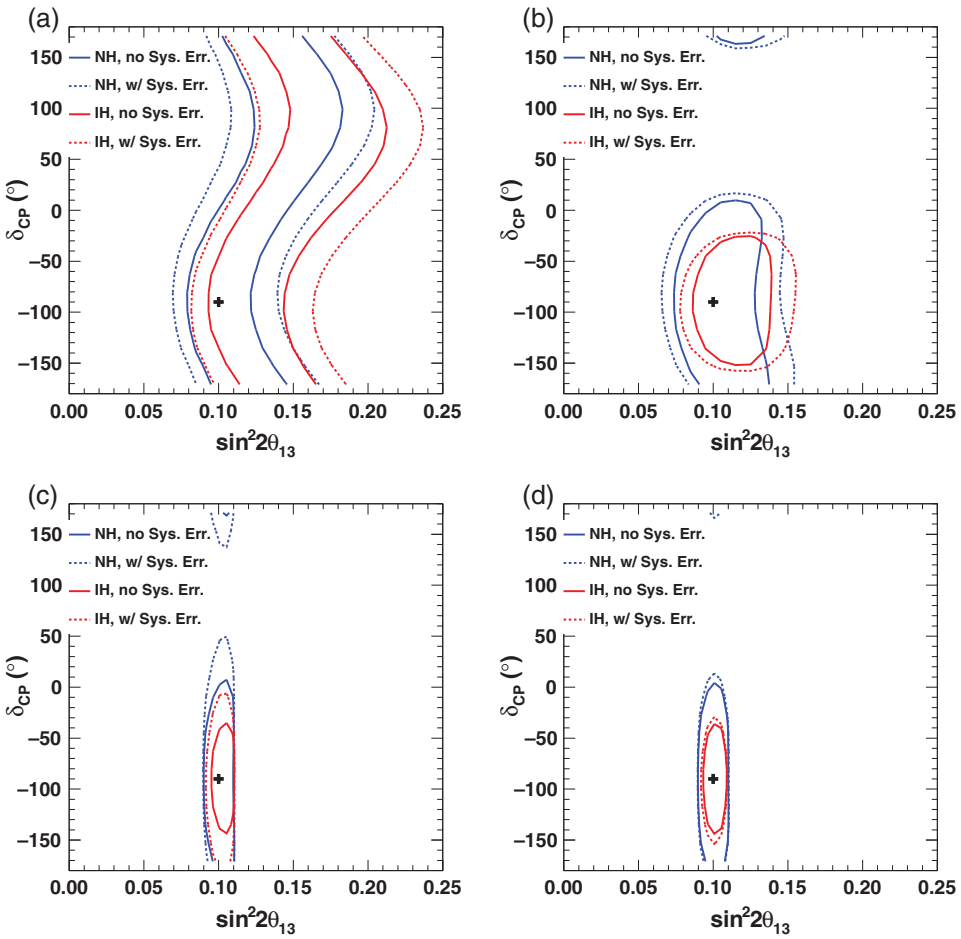

Fig. 5. δ_{CP} vs. $\sin^2 2\theta_{13}$ 90% C.L. intervals for 7.8×10^{21} POT. Contours are plotted for the case of true $\delta_{CP} = -90^\circ$ and NH. The blue curves are fitted assuming the correct MH(NH), while the red are fitted assuming the incorrect MH(IH), and contours are plotted from the minimum χ^2 value for both MH assumptions. The solid contours are with statistical error only, while the dashed contours include the 2012 systematic errors fully correlated between ν- and $\bar{\nu}$-mode. (a) 100% ν-mode. (b) 50% ν-, 50% $\bar{\nu}$-mode. (c) 100% ν-mode, with ultimate reactor constraint. (d) 50% ν-, 50% $\bar{\nu}$-mode, with ultimate reactor constraint.

combined with conservatively projected systematic errors for the full POT. See Sect. 4.5 for details about the projected systematic errors used.

Generally, the effect of the systematic errors is reduced by running with combined ν-mode and $\bar{\nu}$-mode. When running 50% in ν-mode and 50% in $\bar{\nu}$-mode, the statistical 1 σ uncertainty of $\sin^2\theta_{23}$ and Δm^2_{32} is 0.045 and 0.04×10^{-3} eV^2, respectively, at the T2K full statistics.

It should be noted that the sensitivity to $\sin^2\theta_{23}$ shown here for the current exposure (6.57×10^{20} POT) is significantly worse than the most recent T2K result [14], and in fact the recent result is quite close to the final sensitivity (at 7.8×10^{21} POT) shown. This apparent discrepancy comes from three factors. About half of the difference between the expected sensitivity and observed result is due to an apparent statistical fluctuation, where fewer T2K ν_μ events have been observed than expected. Of the remaining difference, half comes from the use of a Feldman–Cousins statistical analysis for the T2K official oscillation result which this sensitivity study does not use. The rest comes from the location of the best-fit point: the expected error depends on the true value of $\sin^2\theta_{23}$ because a local minimum in each octant on each side of the point of maximal disappearance, $\sin^2\theta_{23} \simeq 0.503$ for

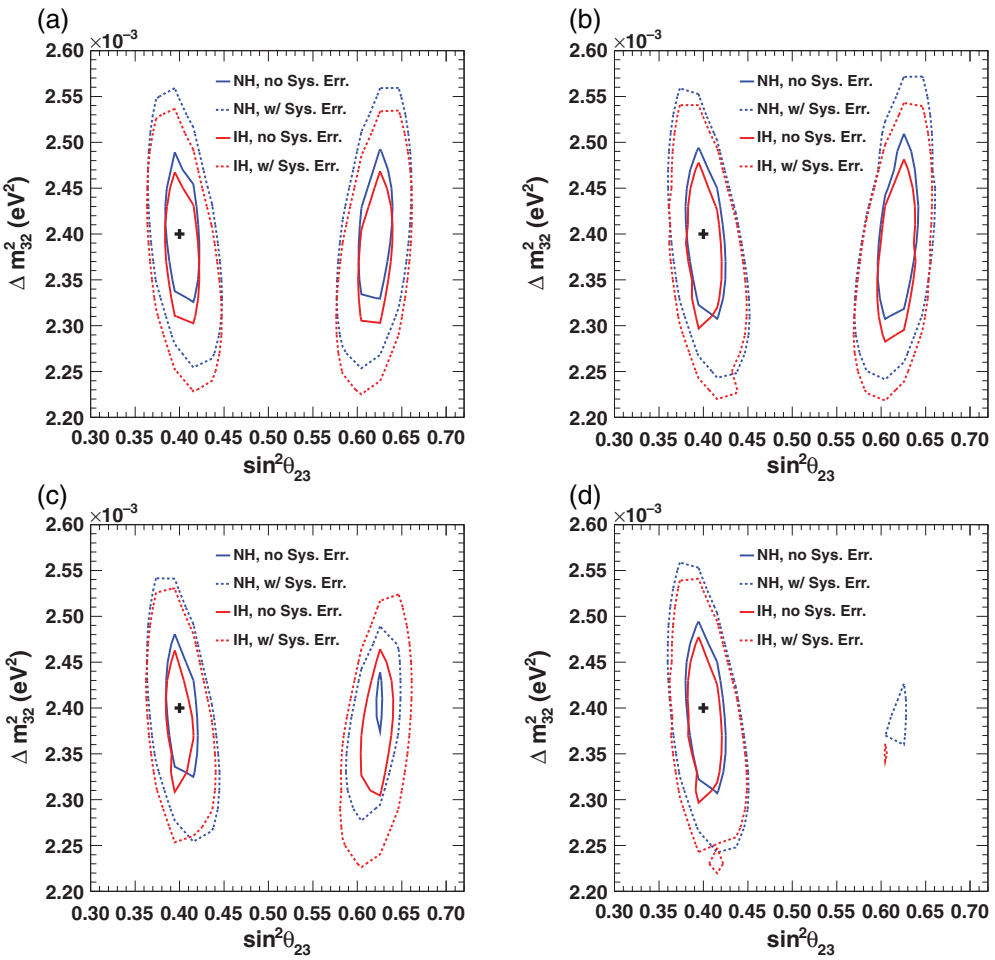

Fig. 6. Δm^2_{32} vs. $\sin^2\theta_{23}$ 90% C.L. intervals for 7.8×10^{21} POT. Contours are plotted for the case of true $\delta_{CP} = 0^\circ$, $\sin^2\theta_{23} = 0.4$, $\Delta m^2_{32} = 2.4 \times 10^{-3}$ eV^2 and NH. The blue curves are fitted assuming the correct MH(NH), while the red are fitted assuming the incorrect MH(IH), and contours are plotted from the minimum χ^2 value for both MH assumptions. The solid contours are with statistical error only, while the dashed contours include the 2012 systematic errors fully correlated between ν- and $\bar{\nu}$-mode. (a) 100% ν-mode. (b) 50% ν-, 50% $\bar{\nu}$-mode. (c) 100% ν-mode, with ultimate reactor error. (d) 50% ν-, 50% $\bar{\nu}$-mode, with ultimate reactor error.

$\sin^2 2\theta_{13} = 0.1$, increases the full width of the $\Delta\chi^2$ curve such that the farther the true point is from maximal disappearance, the larger the error on $\sin^2\theta_{23}$ becomes (where the studies here assume a true value of $\sin^2\theta_{23}$ slightly lower than the point of maximal disappearance, $\sin^2\theta_{23} = 0.5$). Therefore, if results from future running continue to favor maximal disappearance we expect modest improvements in our current constraints, eventually approaching a value close to, and possibly slightly better than, the predicted final sensitivity shown here.

Figure 13 shows the $\sin^2\theta_{23}$ region where maximal mixing or one of the θ_{23} octants can be rejected, as a function of POT in the case of 50% ν- plus 50% $\bar{\nu}$-mode running. Although these plots are made under the condition that the true mass hierarchy is normal and $\delta_{CP} = 0^\circ$, dependence on these conditions is moderate in the case of 50% ν- plus 50% $\bar{\nu}$-mode running.

The sensitivity to reject the null hypothesis $\sin\delta_{CP} = 0$ depends on the true oscillation parameters and is expected to be greatest for the case $\delta_{CP} = +90^\circ$ and inverted MH. Figure 14 shows how the expected $\Delta\chi^2$ evolves as a function of POT in this case, as well as for $\delta_{CP} = -90^\circ$ and normal MH, another case in which the sensitivity is high. These plots indicate the earliest case for T2K to observe

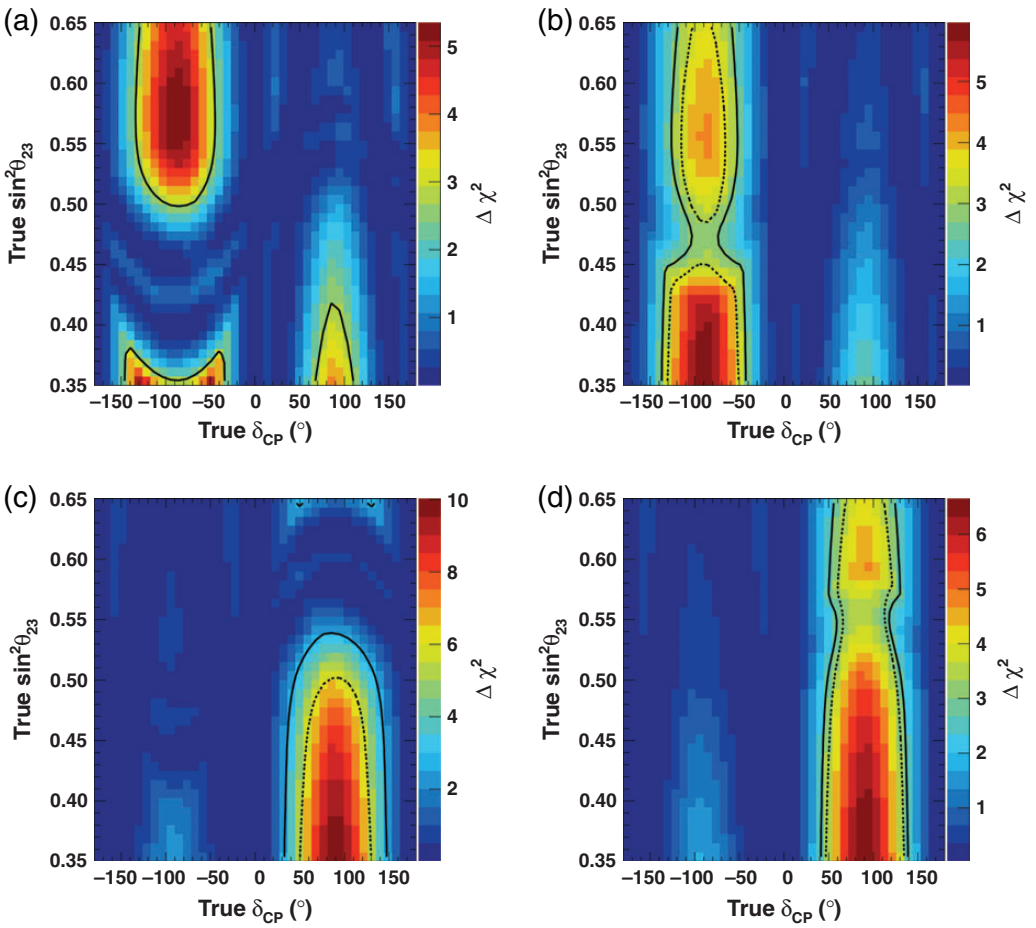

Fig. 7. The expected $\Delta\chi^2$ for the $\sin\delta_{CP} = 0$ hypothesis, in the δ_{CP}–$\sin^2\theta_{23}$ plane. The $\Delta\chi^2$ map shown in color is calculated assuming no systematic errors. The solid contours show the 90% C.L. sensitivity with statistical error only, while the dashed contours include the 2012 T2K systematic error. The dashed contour does not appear in (a) because T2K does not have 90% C.L. sensitivity in this case. (a) Normal mass hierarchy. 100% ν-mode. (b) Normal mass hierarchy. 50% ν-, 50% $\bar{\nu}$-mode. (c) Inverted mass hierarchy. 100% ν-mode. (d) Inverted mass hierarchy. 50% ν-, 50% $\bar{\nu}$-mode.

CP violation. If the systematic error size is negligibly small, T2K may reach a higher sensitivity at an earlier stage by running in 100% ν-mode, since higher statistics are expected in this case. However, with projected systematic errors, 100% ν-mode and 50% ν-mode +50% $\bar{\nu}$-mode running give essentially equivalent sensitivities.

4.5. Effect of reduction of the systematic error size

An extensive study of the effect of the systematic error size was performed. Although the actual effect depends on the details of the errors, here we summarize the results of the study. As given in Table 3, the systematic error on the predicted number of events in Super-K in the 2012 oscillation analysis is 9.7% for the ν_e appearance sample and 13% for the ν_μ disappearance sample.

In Sect. 4.4 we showed the T2K sensitivity with projected systematic errors which are estimated based on a conservative expectation of T2K systematic error reduction. In this case the systematic error on the predicted number of events in Super-K is about 7% for the ν_μ and ν_e samples and about 14% for the $\bar{\nu}_\mu$ and $\bar{\nu}_e$ samples. These errors were calculated by reducing the 2012 oscillation analysis

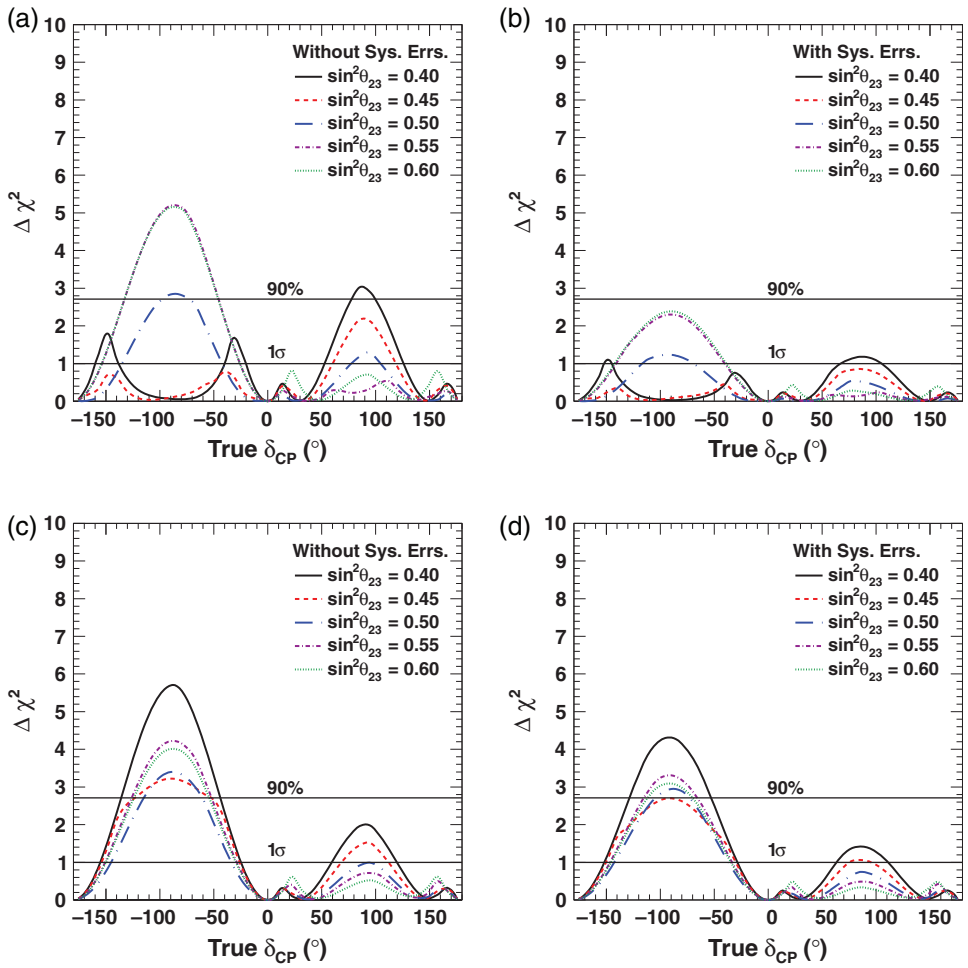

Fig. 8. The expected $\Delta\chi^2$ for the $\sin\delta_{CP} = 0$ hypothesis, plotted as a function of δ_{CP} for various values of $\sin^2\theta_{23}$ (given in the legend) in the case of normal mass hierarchy. (a) 100% ν-mode, statistical error only. (b) 100% ν-mode, with the 2012 systematic errors. (c) 50% ν, 50% $\bar{\nu}$-mode, statistical error only. (d) 50% ν, 50% $\bar{\nu}$-mode, with the 2012 systematic errors.

errors by removing certain interaction model and cross section uncertainties from both the ν_e- and ν_μ-mode errors, and by additionally scaling all ν_μ-mode errors down by a factor of two. Errors for the $\bar{\nu}_\mu$- and $\bar{\nu}_e$-modes were estimated to be twice those of the ν_μ- and ν_e-modes, respectively. These reduced ν-mode errors are in fact very close to the errors used for the oscillation results reported by T2K in 2014, where the T2K oscillation analysis errors have similarly been reduced by improvements in understanding the relevant interactions and cross sections.

For the measurement of δ_{CP}, studies have shown that it is desirable to reduce this to 5% $\sim$ 8% for the ν_e sample and $\sim$10% for the $\bar{\nu}_e$ sample to maximize the T2K sensitivity with full statistics. The measurement of δ_{CP} is nearly independent of the size of the error on the ν_μ and $\bar{\nu}_\mu$ samples as long as we can achieve uncertainty on $\bar{\nu}_\mu$ similar to the current uncertainty on ν_μ. For the measurement of θ_{23} and Δm^2_{32}, the systematic error sizes are significant compared to the statistical error, and the result would benefit from systematic error reduction even for uncertainties as small as 5%.

These error reductions may also be achievable with the implementation of further T2K and external cross section and hadron production measurements, which continue to be made with improved precision.

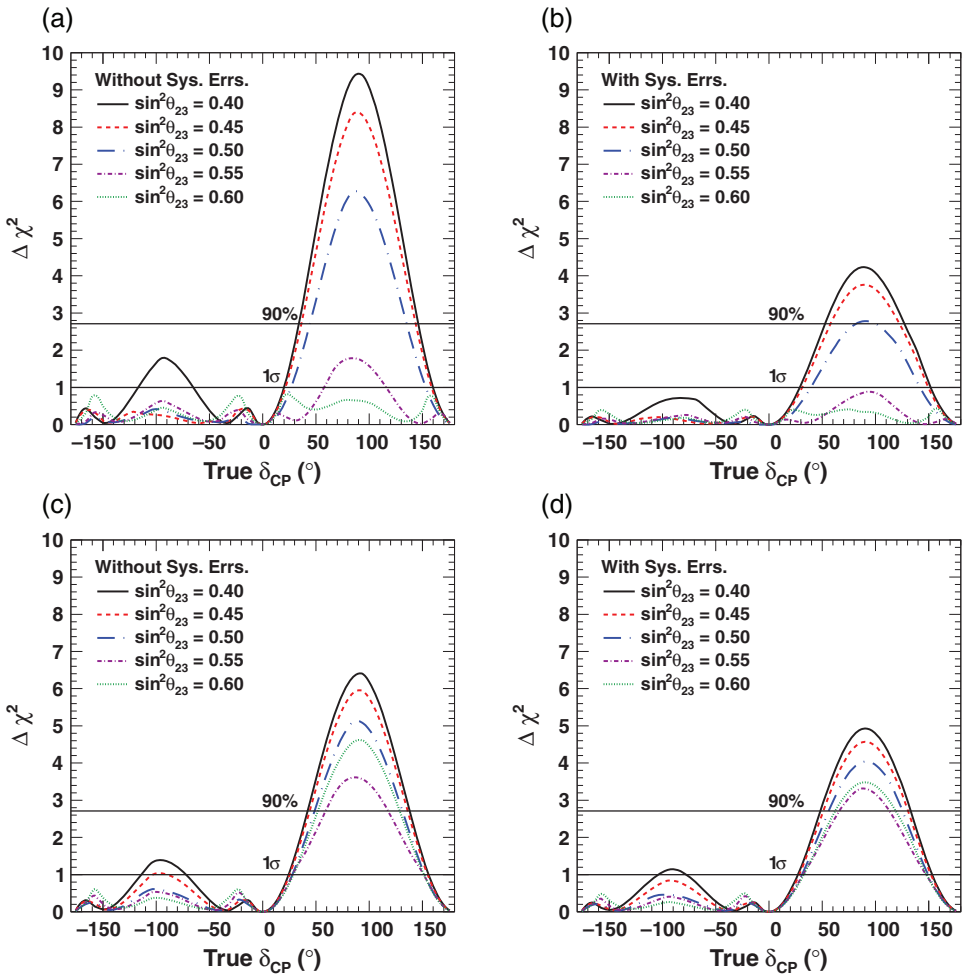

Fig. 9. The expected $\Delta\chi^2$ for the $\sin\delta_{CP} = 0$ hypothesis, plotted as a function of δ_{CP} for various values of $\sin^2\theta_{23}$ (given in the legend) in the case of inverted mass hierarchy. (a) 100% ν-mode, statistical error only. (b) 100% ν-mode, with the 2012 systematic errors. (c) 50% ν, 50% $\bar{\nu}$-mode, statistical error only. (d) 50% ν-, 50% $\bar{\nu}$-mode, with the 2012 systematic errors.

5. T2K and NOνA combined sensitivities

The ability of T2K to measure the value of δ_{CP} (or determine if CPV exists in the lepton sector) is greatly enhanced by the determination of the MH. This enhancement results from the nearly degenerate ν_e appearance event rate predictions at Super-K in the normal hierarchy with positive values of δ_{CP} compared to the inverted hierarchy with negative values of δ_{CP}. Determination of the MH thus breaks the degeneracy, enhancing the δ_{CP} resolution for $\sim$50% of δ_{CP} values. T2K does not have sufficient sensitivity to determine the mass hierarchy by itself. The NOνA experiment [23], which started operating in 2014, has a longer baseline (810 km) and higher peak neutrino energy ($\sim$2 GeV) than T2K. Accordingly, the impact of the matter effect on the predicted far detector event spectra is larger in NOνA $\sim$ 30%) than in T2K ($\sim$10%), leading to a greater sensitivity to the mass hierarchy. Because of the complementary nature of these two experiments, better constraints on the oscillation parameters, δ_{CP}, $\sin^2\theta_{23}$, and the MH can be obtained by comparing the $\nu_\mu \to \nu_e$ oscillation probability of the two experiments. To evaluate the benefit of combining the two experiments, we have developed a code based on GLoBES [38,39]. The studies using projected T2K and NOνA data

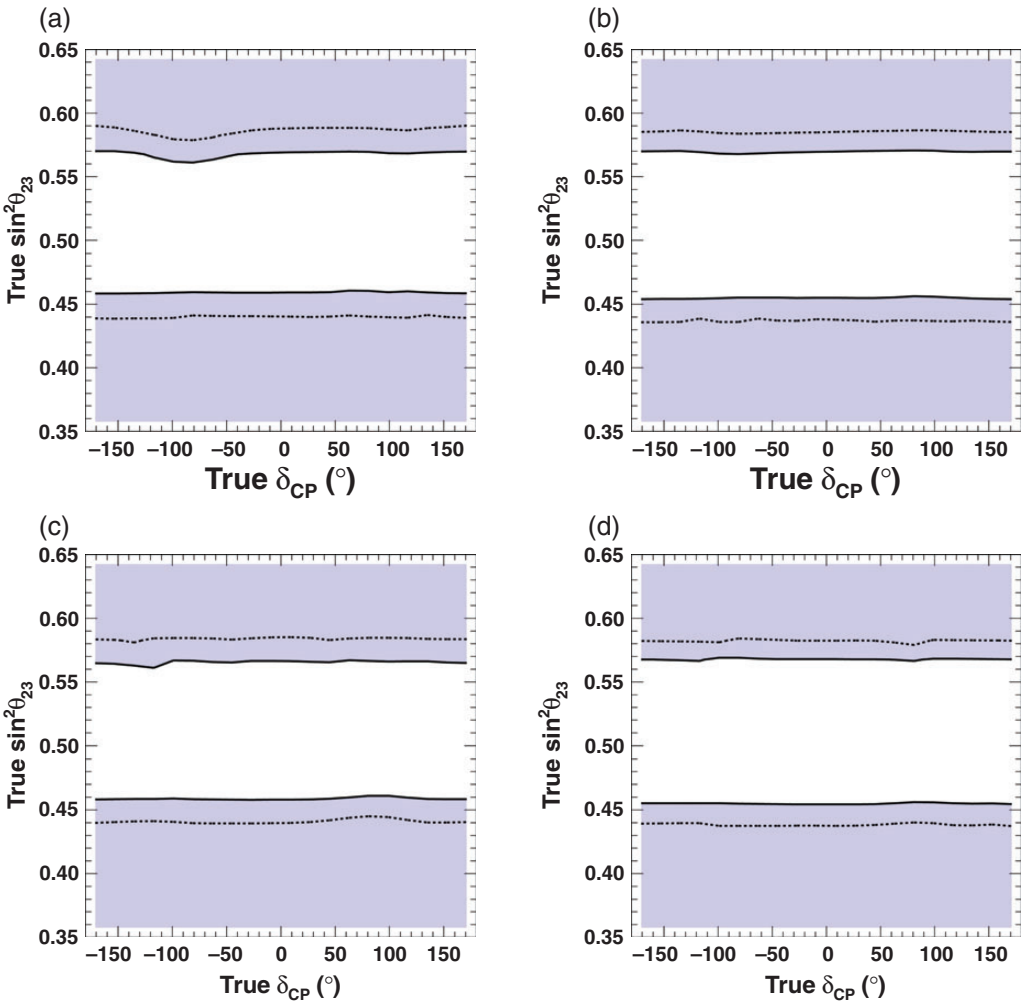

Fig. 10. The region, shown as a shaded area, where T2K has more than a 90 % C.L. sensitivity to reject maximal mixing. The shaded region is calculated assuming no systematic errors (the solid contours show the 90% C.L. sensitivity with statistical error only), and the dashed contours show the sensitivity including the 2012 systematic errors. (a) Normal mass hierarchy. 100% ν-mode. (b) Normal mass hierarchy. 50% ν-, 50% $\bar{\nu}$-mode. (c) Inverted mass hierarchy. 100% ν-mode (d) Inverted mass hierarchy. 50% ν-, 50% $\bar{\nu}$-mode.

samples show the full physics reach for the two experiments, individually and combined, along with studies aimed at optimization of the ν-mode to $\bar{\nu}$-mode running ratios of the two experiments.

Figure 15 shows the relation between the expected number of events of T2K and NOνA for various values of δ_{CP}, $\sin^2\theta_{23}$, and mass hierarchies. The NH and IH predictions occupy distinct regions in the plot suggesting how a combined analysis T2K–NOνA fit leads to increased sensitivity. However, this plot does not include the (statistical + systematic) uncertainties on measurements of these event rates. This would result in regions of overlap where the MH cannot be determined, and the sensitivity to δ_{CP} is degraded. In order to evaluate the effect of combining the results from T2K and NOνA quantitatively, we have conducted a T2K–NOνA combined sensitivity study. The GLoBES [38,39] software package was used to fit oscillation parameters based on the reconstructed neutrino energy spectra of the two experiments. The fits were conducted by minimizing $\Delta\chi^2$ which is calculated from spectra generated with different sets of oscillation parameters, and includes penalty terms for deviations of the signal and background normalizations from nominal. The best-fit $\Delta\chi^2$ calculated

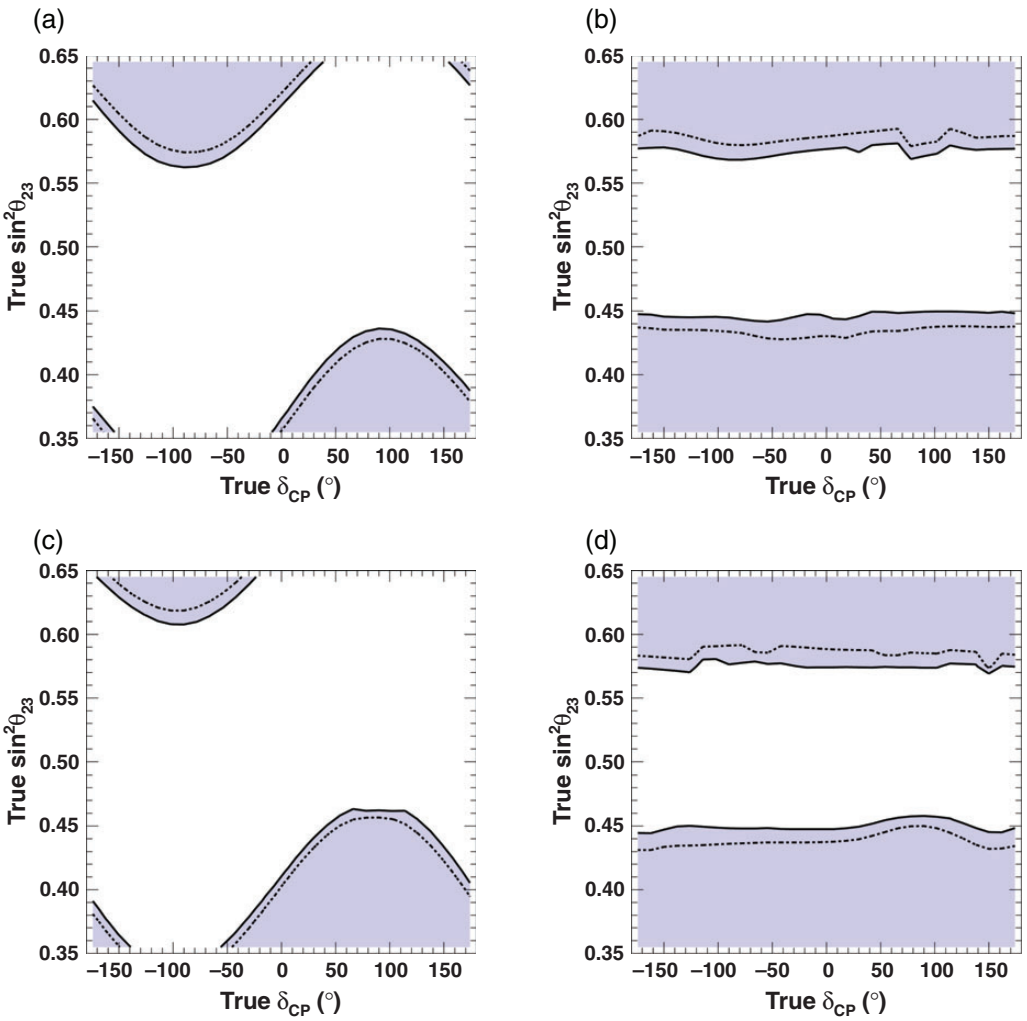

Fig. 11. The region, shown as a shaded area, where T2K has more than a 90% C.L. sensitivity to reject one of the octants of θ_{23}. The shaded region is calculated assuming no systematic errors (the solid contours show the 90% C.L. sensitivity with statistical error only), and the dashed contours show the sensitivity including the 2012 T2K systematic errors. (a) Normal mass hierarchy. 100% ν-mode. (b) Normal mass hierarchy. 50% ν-, 50% $\bar{\nu}$-mode. (c) Inverted mass hierarchy. 100% ν-mode. (d) Inverted mass hierarchy. 50% ν-, 50% $\bar{\nu}$-mode.

by GLoBES was the metric chosen to characterize sensitivity, as it is related to the probability that a given data set can result from two different hypotheses.

GLoBES combines flux, cross section, energy resolution/bias, and efficiency information for an experiment to estimate energy spectra of neutrino interaction samples used for analyses. Then GLoBES uses a full three-flavor oscillation probability formulation to fit analysis spectra generated assuming different oscillation parameters to each other (varying oscillation parameter values and parameters accounting for systematic uncertainties within their uncertainties). The oscillation parameters, unless otherwise stated, are those shown in Table 2. The GLoBES three-flavor analysis package works very similarly to the fitter used for the studies presented in Sect. 4. Several validation studies were done to ensure that the two methods produced the same results when given the same inputs.

The T2K, NOνA, and combined sensitivities were generated using a modified version of GLoBES that allowed for use of inputs generated from Monte Carlo simulations of T2K neutrino interactions

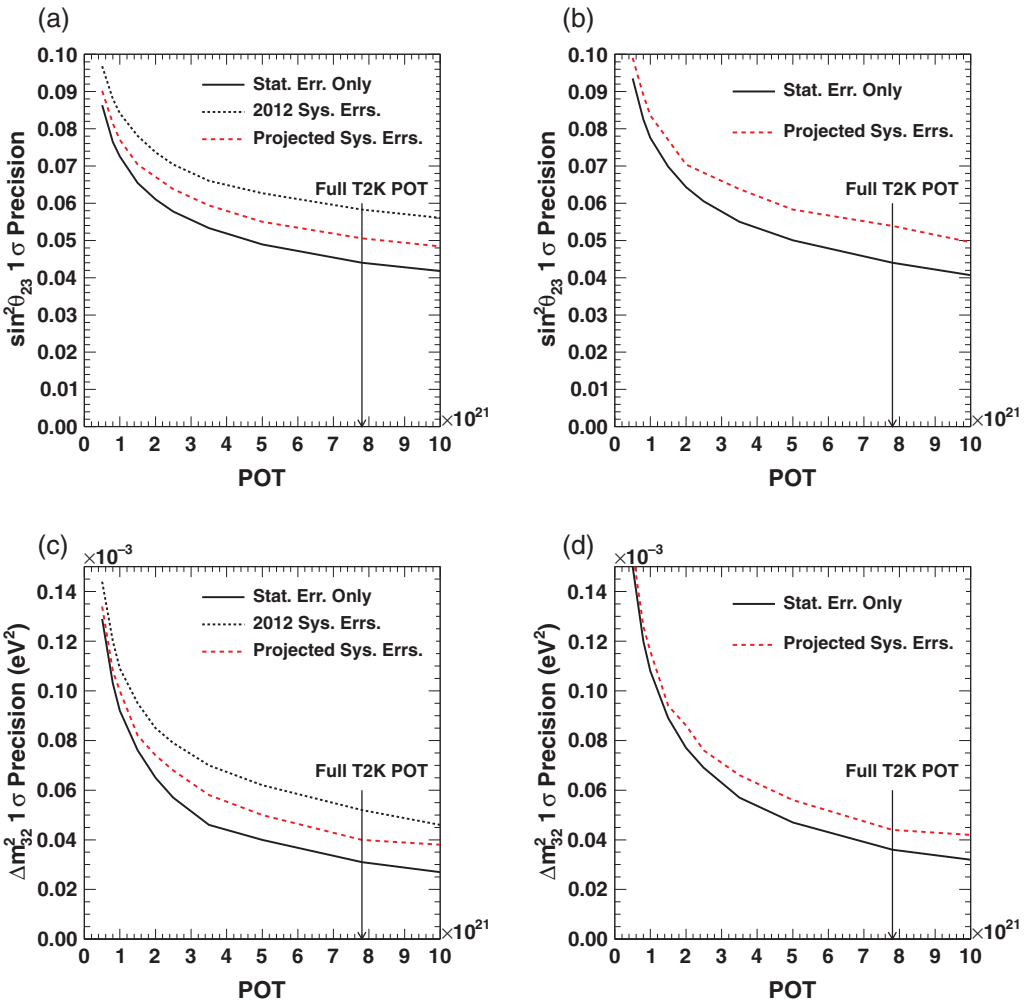

Fig. 12. The uncertainty on $\sin^2\theta_{23}$ and Δm^2_{32} plotted as a function of T2K POT. Plots assume the true oscillation parameters given in Table 2. The solid curves include statistical errors only, while the dashed curves assume the 2012 systematic errors (black) or the projected systematic errors (red). A constraint based on the ultimate reactor precision is included. (a) 100% ν-mode. (b) 50% ν, 50% $\bar{\nu}$-mode. (c) 100% ν-mode. (d) 50% ν, 50% $\bar{\nu}$-mode.

in the Super-Kamiokande detector. The inputs describing the NOνA experiment were developed in conjunction with NOνA collaborators, and validated against official NOνA sensitivity plots.[3] We assume the same run plan as presented in NOνA's TDR: 1.8×10^{21} POT for ν and 1.8×10^{21} POT for $\bar{\nu}$ modes, corresponding to three years of running in each mode.

The GLoBES inputs defining the analysis sample acceptances for the signal, the NC background, the ν_μ CC background, and the ν_e CC background were tuned to match this official event rate prediction from NOνA. For example, Table 6 summarizes the expected number of ν_e appearance events for NOνA[4] when $\sin^2 2\theta_{13} = 0.95$ is assumed and the solar oscillation terms or matter effects in the oscillation probability are neglected.

[3] http://www-nova.fnal.gov/plots_and_figures/plot_and_figures.html;
http://nova-docdb.fnal.gov/cgi-bin/ShowDocument?docid=7546;
http://nova-docdb.fnal.gov/cgi-bin/ShowDocument?docid=7552.
[4] http://nova-docdb.fnal.gov/cgi-bin/ShowDocument?docid=7552.

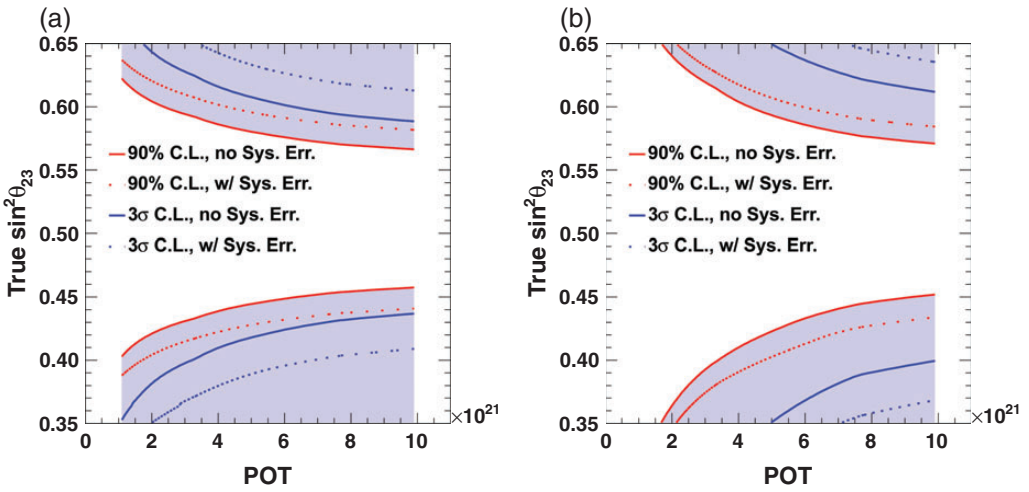

Fig. 13. The region where maximal mixing or one θ_{23} octant can be rejected at the stated confidence levels (given by the shaded region), as a function of POT in the case of 50% ν-, 50% $\bar{\nu}$-mode. These plots are made under the condition that the true mass hierarchy is normal and $\delta_{CP} = 0$. The dashed contours include the 2012 systematic errors fully correlated between ν and $\bar{\nu}$. A constraint based on the ultimate reactor precision is included. (a) $\theta_{23} \neq \pi/4$. (b) θ_{23} octant.

Since NOνA has only recently begun taking data, detailed evaluation of systematic uncertainties is not yet published. Therefore, the combined sensitivity studies used a simplified systematics treatment for both T2K and NOνA: a 5% normalization uncertainty on signal events and a 10% normalization uncertainty on background events for both appearance and disappearance spectra. Uncertainties that impact the spectral shape are not considered. This is a reasonable choice since both experiments use a narrow-band beam and much of the oscillation sensitivity comes from the measured event rates. The uncertainties are assumed to be uncorrelated for ν_e appearance, $\bar{\nu}_e$ appearance, ν_μ disappearance, and $\bar{\nu}_\mu$ disappearance. This simple systematics implementation, referred to in the rest of the paper as "normalization systematics," is the same as that adopted in the NOνA TDR and is also a reasonable representation of the projected uncertainties at T2K. The sensitivities shown here are obtained assuming $\sin^2 2\theta_{13} = 0.1$ with the projected reactor constraint of 5%.

When determining the MH, $\Delta\chi^2$ is not distributed according to a χ^2 distribution because the MH is a discrete, rather than a continuous, variable. Toy MC studies, where many pseudo-experiments are generated with statistical and systematic fluctuations, were used to evaluate the validity of applying a $\Delta\chi^2$ test statistic, as given in Eq. (5), for the MH determination.

The left column of Fig. 16 shows distributions for a test static for $H_0 =$ IH:

$$T = \chi^2_{\mathrm{IH}} - \chi^2_{\mathrm{NH}}, \tag{6}$$

where χ^2_{IH} and χ^2_{NH} are the minimum χ^2 values obtained by fitting the oscillation parameters while fixing the MH to the inverted or normal mass hierarchy, respectively. This T is plotted here instead of $\Delta\chi^2$ for easier interpretation. In the figure, the blue (red) distributions are for the case where test or "observed" spectra were generated for the inverted (normal) mass hierarchy with statistical and systematic fluctuations. Except for δ_{CP}, the test oscillation parameters were fixed to the nominal values given in Table 2. The value of δ_{CP} was fixed to that given in each caption for the NH, while it was thrown over all values of δ_{CP} for the IH. This is done in order to calculate the p-value for $H_0 =$ IH with unknown δ_{CP} when the test point is in the NH [40]. The right column of Fig. 16 is the

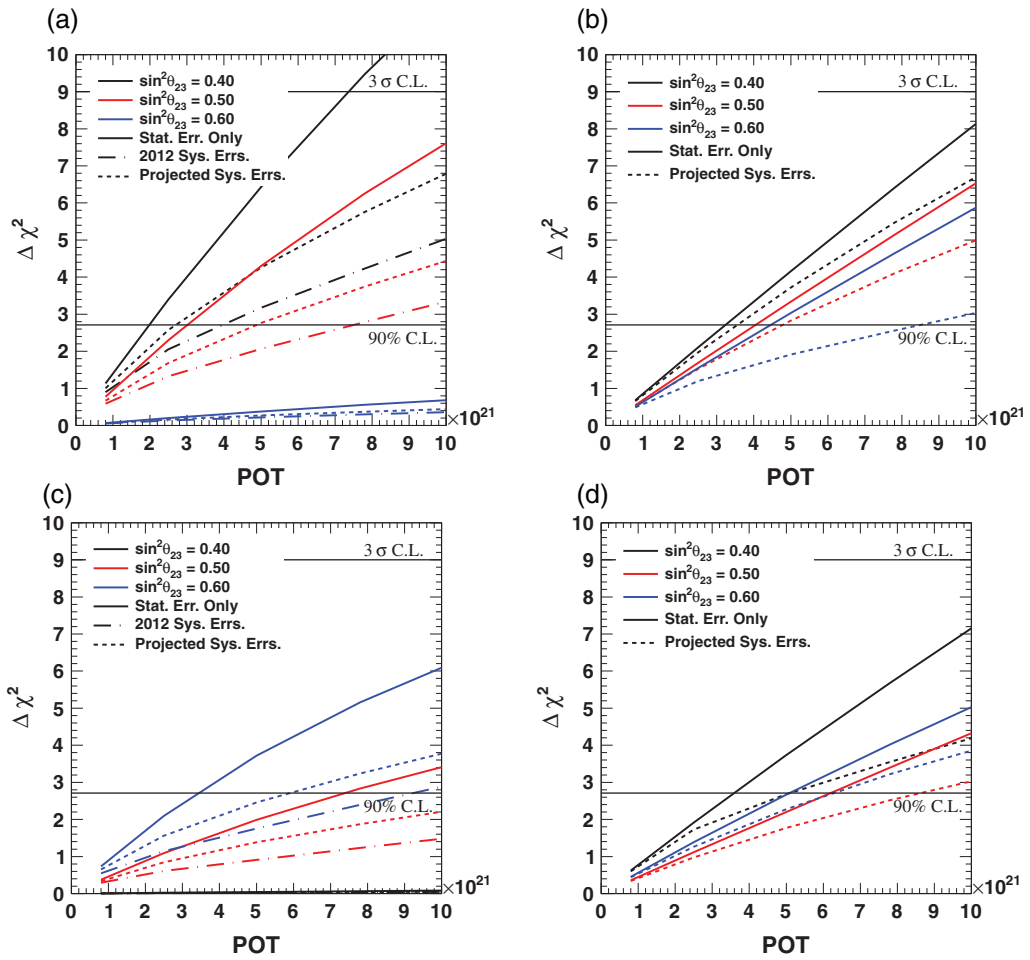

Fig. 14. The expected $\Delta\chi^2$ for the $\sin\delta_{CP} = 0$ hypothesis, plotted as a function of POT. Plots assume true $\sin^2 2\theta_{13} = 0.1$, various true values of $\sin^2\theta_{23}$ (as given in the plot legends), and δ_{CP} and the MH as given in the figure captions. The solid curves include statistical errors only, while the dash-dotted (dashed) curves assume the 2012 systematic errors (the projected systematic errors). Note that the sensitivity heavily depends on the assumed conditions, and that the conditions applied for these figures correspond to the cases where the sensitivity for $\sin\delta_{CP} \neq 0$ is maximal. (a) 100% ν-mode, $\delta_{CP} = 90^\circ$, IH. (b) 50% ν-, 50% $\bar{\nu}$ running, $\delta_{CP} = 90^\circ$, IH. (c) 100% ν-mode, $\delta_{CP} = 90^\circ$, NH. (d) 50% ν-, 50% $\bar{\nu}$ running, $\delta_{CP} = 90^\circ$, NH.

same, but with the opposite MH hypothesis test ($H_0 =$ NH):

$$T = \chi^2_{\mathrm{NH}} - \chi^2_{\mathrm{IH}} \tag{7}$$

with a test point in the IH. The T-value calculated using the spectrum generated from the MC sample statistical mean (T_{MC}), which is generally used in this paper, is compared with the median T-value for the ensemble of toy MC experiments (T_{median}) in Table 7 for different oscillation parameter sets. The p-values calculated for T_{MC}, assuming that $\Delta\chi^2$ follows a true χ^2 distribution, compared with the p-values calculated as the fraction of the T distribution for $H_0 =$ (correct MH) above T_{median} are also given.

Figures 17 through 19 show plots of expected C.L. contours for T2K, NOνA, and T2K–NOνA combined fits as functions of $\sin^2\theta_{23}$ vs. δ_{CP}. Regions where $\sin\delta_{CP} = 0$, one MH, and one θ_{23} octant are expected to be ruled out at the 90% C.L. are shown. Significantly wider regions are covered by combining the results from T2K and NOνA.

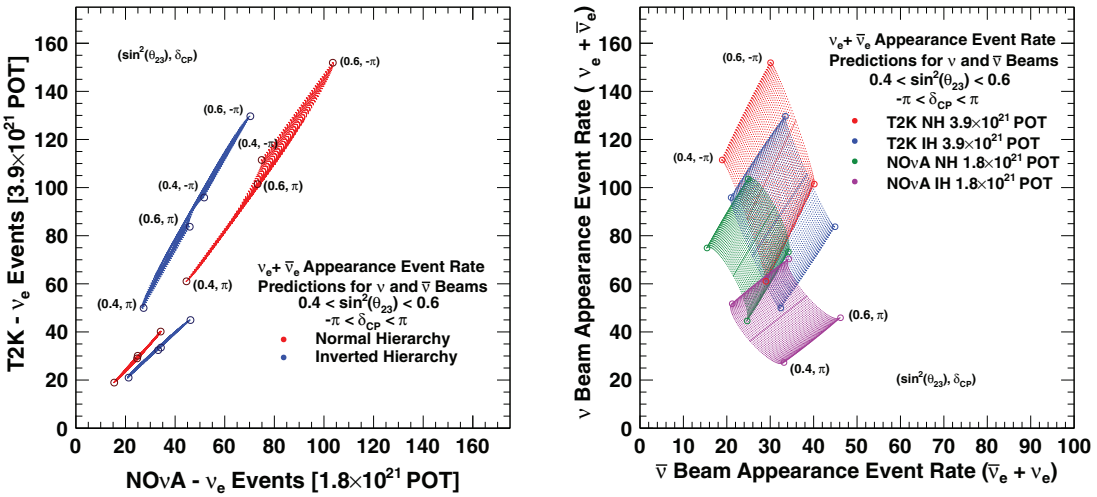

Fig. 15. Relation between the expected number of $\nu_e + \bar{\nu}_e$ signal events produced by neutrino-mode running and antineutrino-mode running in T2K and NOνA, for various values of δ_{CP}, $\sin^2\theta_{23}$, and mass hierarchy. In the plot of predicted T2K rate versus the predicted NOνA rate (left) the blue (IH) and red (NH) upper bands are for neutrino-mode running while the red (NH) and blue (IH) bottom bands are for the antineutrino-mode running. The predicted number of $\nu_e + \bar{\nu}_e$ events produced in neutrino-mode running versus events produced in antineutrino-mode running (right) are shown for T2K in red (NH) and blue (IH), and for NOνA in green (NH) and magenta (IH). Representative points at the edges of the δ_{CP} and $\sin^2\theta_{23}$ ranges are highlighted. Systematic and statistical uncertainties are not included.

Table 6. Expected number of ν_e appearance signal and background events for NOνA at 1.8×10^{21} POT for each of the ν and $\bar{\nu}$ modes.* The oscillation probabilities used to calculate the predicted number of events assumed $\sin^2 2\theta_{13} = 0.095$ and do not include the solar oscillation terms or matter effects.

Beam	Signal	NC Bkg	ν_μ CC	ν_e CC	Total Bkg
ν-mode	72.6	20.8	5.2	8.4	34.5
$\bar{\nu}$-mode	33.8	10.6	0.7	5.0	16.3

*http://nova-docdb.fnal.gov/cgi-bin/ShowDocument?docid=7552.

In Figures 20 and 21 the $\Delta\chi^2$ for $\sin\delta_{CP} = 0$ and for each MH is plotted as a function of "true" δ_{CP} in the case of $\sin^2(\theta_{23}) = 0.5$. The "true" value of $\sin^2(\theta_{23}) = 0.5$ was chosen to present a simplified view of the sensitivities for maximal mixing. The T2K's $\Delta\chi^2$ is smaller at $\delta_{CP} = +90°(-90°)$ compared to that at the opposite sign of $\delta_{CP} = -90°(+90°)$ for the NH (IH) case while those are similar for NOνA. This comes from the large degeneracy between the CP-violating term and the matter effect for T2K. In the case of NOνA, the matter effect is large enough that the degenerate parameters space is much smaller, as can be seen in Fig. 15. The complex structure for positive (negative) values of δ_{CP} with a true NH (IH) is also due to the fact that $\Delta\chi^2$ calculation profiles over MH, and the expected number of ν_e appearance events, is nearly degenerate in these regions. T2K would perform better than or comparable to NOνA if the MH was assumed to be known. However, there is no experiment, besides NOνA, that expects to determine the MH on the relevant time scale, thus the case of a known MH is not presented. These figures demonstrate the sensitivity of the two experiments, as well as the benefit of combined analysis of the two data sets on the ability to determine MH and CPV.

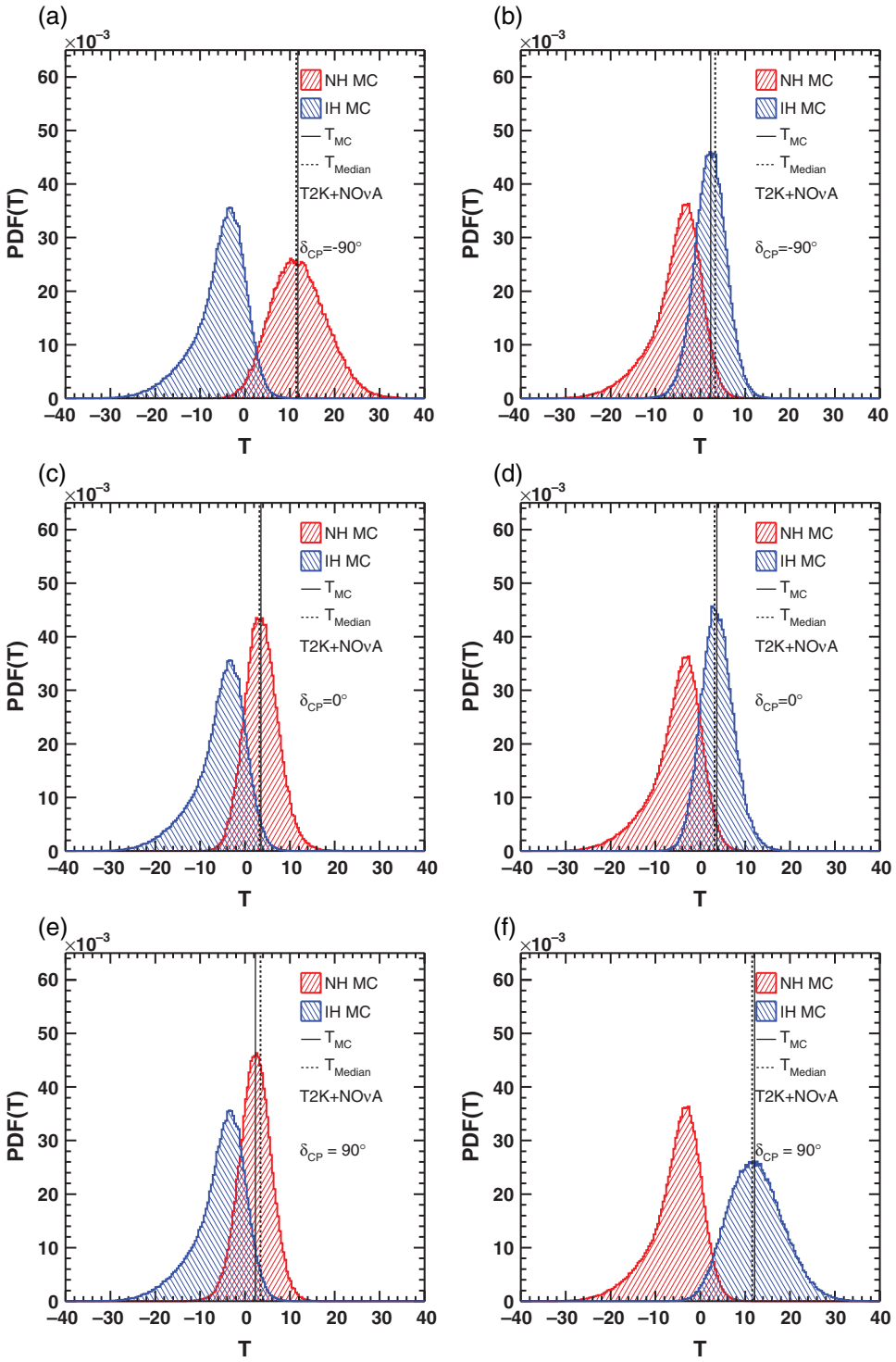

Fig. 16. Distributions of the test statistic, T, for toy MC experiments with the null hypothesis $H_0 =$ I(N)H are shown in the left (right) column. Toy MC experiments are generated with the nominal oscillation parameters except for the MH and δ_{CP}; those generated with NH are indicated in red and those with IH in blue. The value of δ_{CP} is fixed to the value indicated in the sub-captions when $H_0 =$ (correct MH), but thrown when $H_0 =$ (incorrect MH), where the correct MH is also given in the sub-captions. Solid lines indicate the value of the MH determination sensitivity metric used in this paper (calculated using the spectra at the MC sample statistical mean), and dashed lines indicate the T-value for the median of the toy MC distribution. (a) $\delta_{CP} = -90^\circ$, NH. (b) $\delta_{CP} = -90^\circ$, IH. (c) $\delta_{CP} = 0^\circ$, NH. (d) $\delta_{CP} = 0^\circ$, IH. (e) $\delta_{CP} = 90^\circ$, NH. (f) $\delta_{CP} = 90^\circ$, IH.

Table 7. Values of $T_{\rm MC}$ and $T_{\rm median}$ and their associated p-values. The T-values correspond to the vertical lines shown in Fig. 16. The p-values are computed either with a χ^2 distribution for one degree of freedom from the spectra at the toy MC statistical mean or using an ensemble of toy MC experiments.

	by MC mean spectra		by toy MC experiments	
	$T_{\rm MC}$	p-value(χ^2)	$T_{\rm median}$	p-value(toy MC)
NH, $\delta_{\rm CP} = -90^\circ$	11.4	0.00073	11.8	0.000065
NH, $\delta_{\rm CP} = 0^\circ$	3.22	0.073	3.57	0.019
NH, $\delta_{\rm CP} = +90^\circ$	3.47	0.063	2.34	0.040
IH, $\delta_{\rm CP} = -90^\circ$	3.33	0.068	2.30	0.042
IH, $\delta_{\rm CP} = 0^\circ$	3.19	0.074	3.79	0.015
IH, $\delta_{\rm CP} = +90^\circ$	11.6	0.00067	12.5	0.000031

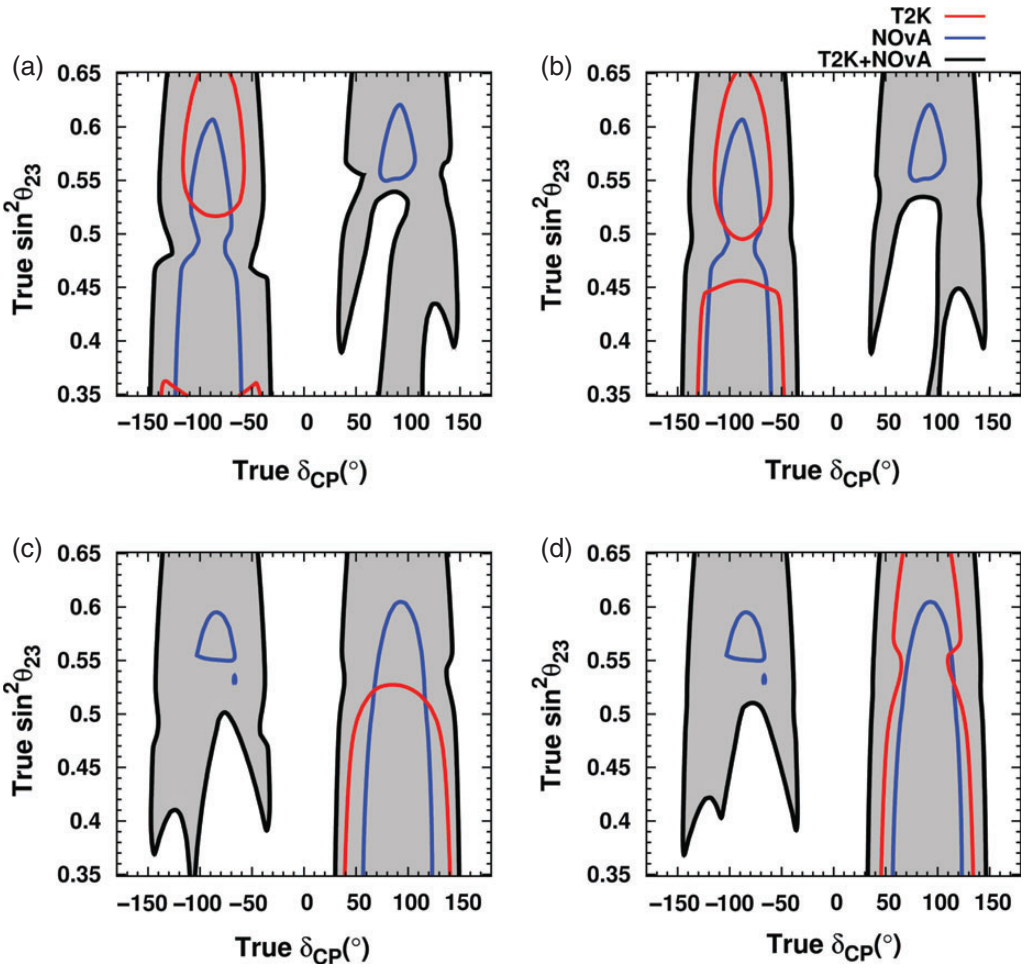

Fig. 17. Regions where T2K (red), NOνA (blue), and T2K + NOνA (black) are predicted to rule out $\sin\delta_{\rm CP} = 0$ at 90% C.L. Points within the gray regions are where $\sin\delta_{\rm CP} = 0$ is predicted to be rejected at 90% C.L. for T2K + NOνA, assuming simple normalization systematics as described in the text. (a) 1:0 T2K, 1:1 NOνA ν:$\bar{\nu}$, NH. (b) 1:1 T2K, 1:1 NOνA ν:$\bar{\nu}$, NH. (c) 1:0 T2K, 1:1 NOνA ν:$\bar{\nu}$, IH. (d) 1:1 T2K, 1:1 NOνA ν:$\bar{\nu}$, IH.

6. Neutrino-mode and antineutrino-mode running time optimization

As previously shown in Sect. 4, a significant fraction of $\bar{\nu}$-mode running improves the sensitivity to CP violation, especially when systematic uncertainties are taken into account. In this section studies

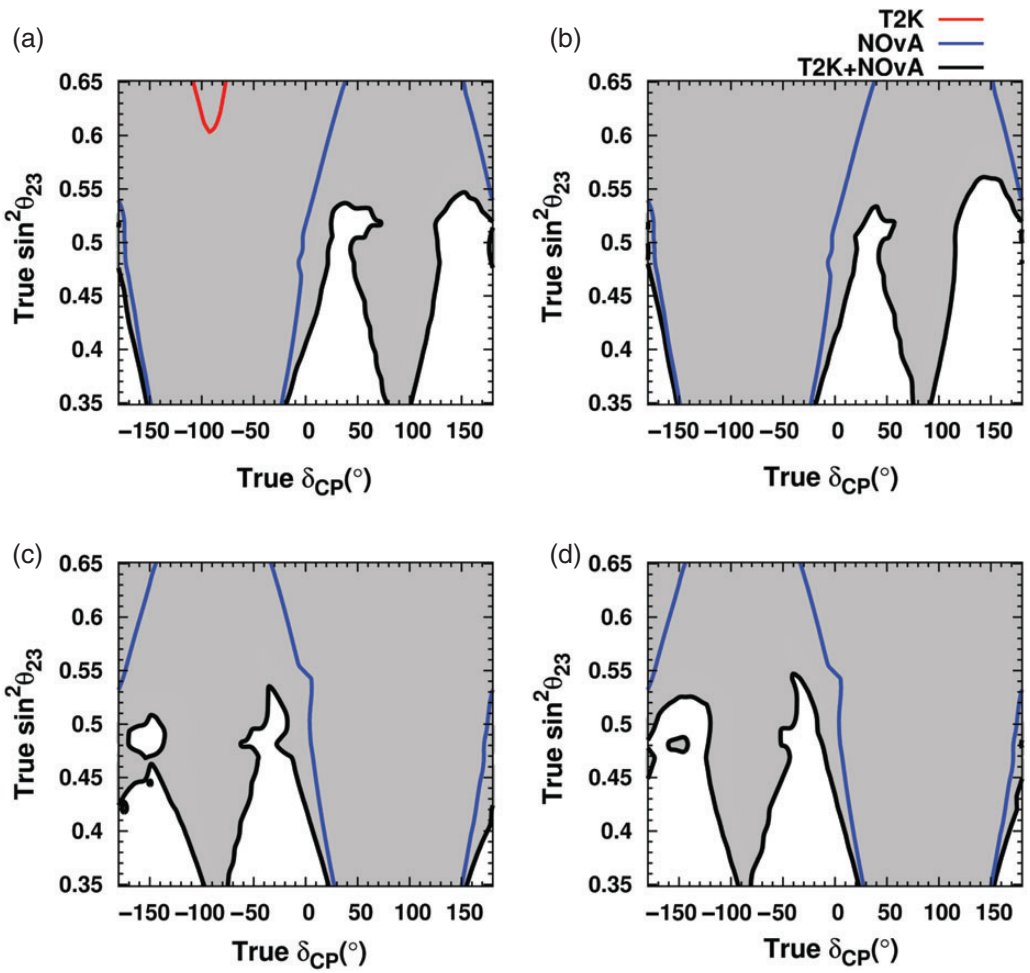

Fig. 18. Regions for T2K (red), NOνA (blue), and T2K + NOνA (black) where the incorrect mass hierarchy is predicted to be rejected at 90% C.L. Points within the gray regions are where the incorrect mass hierarchy is predicted to be rejected at 90% C.L. for T2K + NOνA, assuming simple normalization systematics as described in the text. (a) 1:0 T2K, 1:1 NOνA ν:$\bar{\nu}$, NH. (b) 1:1 T2K, 1:1 NOνA ν:$\bar{\nu}$, NH. (c) 1:0 T2K, 1:1 NOνA ν:$\bar{\nu}$, IH. (d) 1:1 T2K, 1:1 NOνA ν:$\bar{\nu}$, IH.

of the ν:$\bar{\nu}$ running ratios are shown for T2K, NOνA, and combined fits of T2K + NOνA simulated data using the tools developed in Sect. 5. A set of metrics is defined that characterizes the ability of each experiment or a combined fit of both experiments to constrain δ_{CP}, reject $\delta_{CP} = 0$, or determine the MH. The following metrics are used in these studies:

- δ_{CP} half-width: The 1 σ half-width is defined as half of the 1 σ Confidence Interval (C.I.) about the true value of δ_{CP}. In some cases there are degenerate 1 σ C.I. regions in δ_{CP} that are disconnected from the central value. In this case half of the width of the degenerate region is added to this metric. This is a measure of the precision that can be acheived in measurment of δ_{CP}.
- Median $\Delta\chi^2$ for $\delta_{CP} = 0$: This metric defines the $\Delta\chi^2$ value for which 50% of true δ_{CP} values can be distinguished from $\delta_{CP} = [0, \pi]$. This is a measure of sensitivity to CPV.
- Lowest $\Delta\chi^2$ for mass hierarchy determination: This metric defines the $\Delta\chi^2$ value at which the mass hierarchies can be distinguished for 100% of true δ_{CP} values.

Each metric is calculated for a T2K + NOνA combined analysis for various ν:$\bar{\nu}$ run ratios. Figure 22 gives the lowest $\Delta\chi^2$ values for mass hierarchy determination for ν:$\bar{\nu}$ variations in a

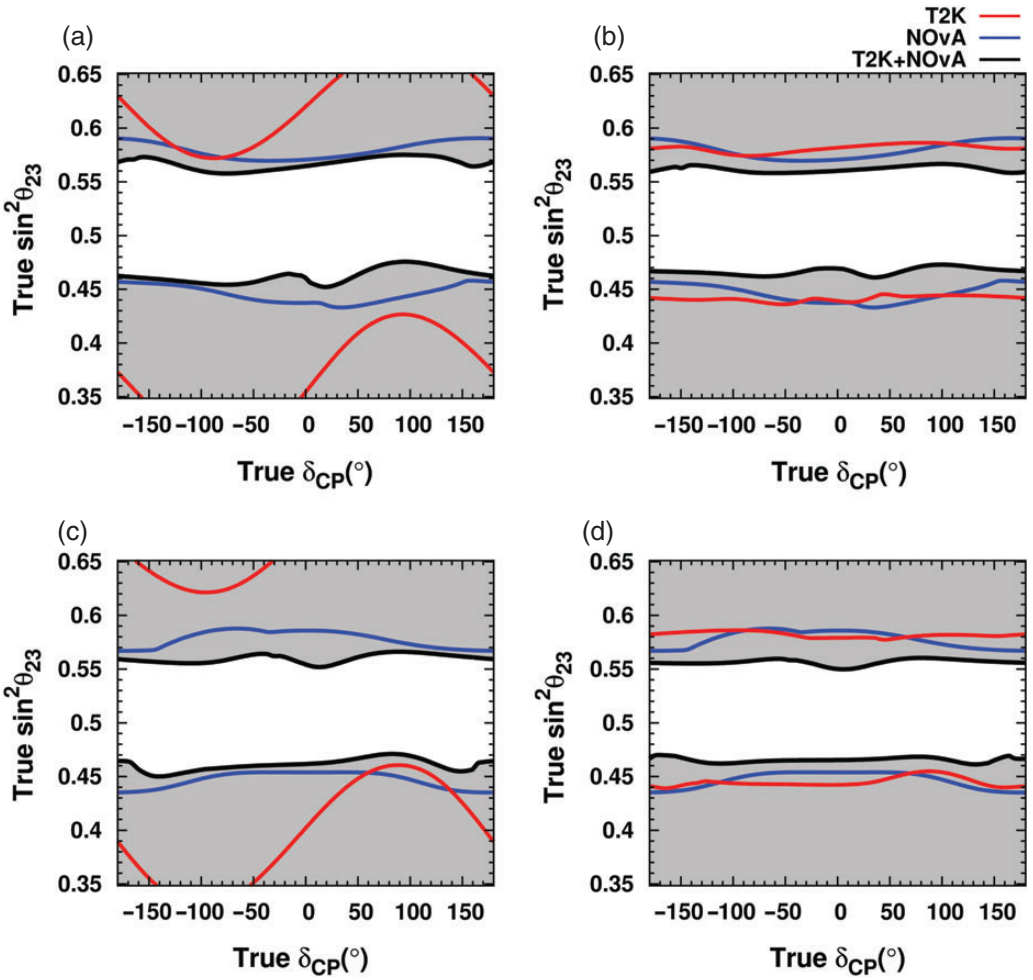

Fig. 19. Regions for T2K (red), NOνA (blue), and T2K + NOνA (black) where the incorrect octant is predicted to be rejected at 90% C.L. Points inside the gray regions are where the incorrect octant is predicted to be rejected at 90% C.L. for T2K + NOνA assuming simple normalization systematics as described in the text. (a) 1:0 T2K, 1:1 NOνA ν:$\bar{\nu}$, NH. (b) 1:1 T2K, 1:1 NOνA ν:$\bar{\nu}$, NH. (c) 1:0 T2K, 1:1 NOνA ν:$\bar{\nu}$, IH. (d) 1:1 T2K, 1:1 NOνA ν:$\bar{\nu}$, IH.

combined T2K + NOνA fit. They are computed from the results of studies like the one shown in Fig. 21 and conservatively summarize the content of the plot in one data point. For example, the lowest $\Delta\chi^2$ value for mass hierarchy determination at 1:0 (100% ν running) T2K, 5:5 (50% ν/50% $\bar{\nu}$ running) NOνA running is the lowest $\Delta\chi^2$ from Fig. 21(a) ($\Delta\chi^2 = 2.19$).

Similarly, Fig. 23 gives the median $\Delta\chi^2$ values for $\sin\delta_{CP} = 0$ for ν:$\bar{\nu}$ variations in a combined T2K + NOνA fit. These values are computed from studies like the ones presented in Fig. 20. The $\sin\delta_{CP} = 0$ median $\Delta\chi^2$ value at 1:0 T2K, 5:5 NOνA running is the median $\Delta\chi^2$ from Fig. 20(a) ($\Delta\chi^2 = 2.6$).

Figure 24 summarizes the data in Fig. 22 and compares it with the metric calculated for T2K-only running. The black curve gives the lowest $\Delta\chi^2$ for MH determination in a combined, T2K + NOνA, fit as a function of T2K ν:$\bar{\nu}$ running ratio with the NOνA running fixed at 1:1. As shown previously, the T2K data set alone has almost no sensitivity to the MH determination. The curves for 5:5 NOνA running with systematics (black dashed) shows an optimal T2K running ratio of around 6:4 for a combined fit. However, the metric is very flat with respect to the T2K ν:$\bar{\nu}$ run ratio for ν running

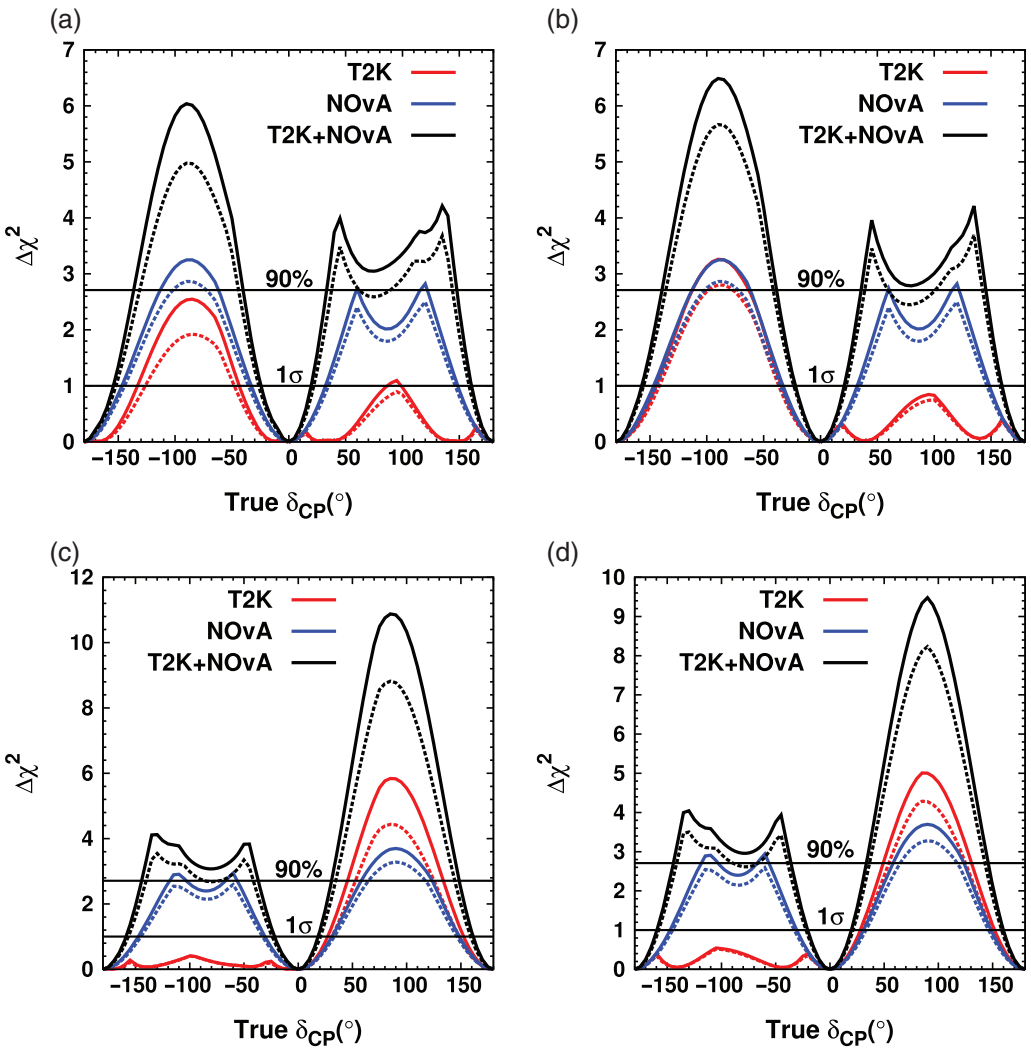

Fig. 20. The predicted $\Delta\chi^2$ for rejecting the $\sin\delta_{CP} = 0$ hypothesis, as a function of δ_{CP} for T2K (red), NOνA (blue), and T2K + NOνA (black). Dashed (solid) curves indicate studies where normalization systematics are (not) considered. The "true" value of $\sin^2(\theta_{23})$ is assumed to be 0.5, and the "true" MH is assumed to be the NH (top) or the IH (bottom). The "test" MH is unconstrained. (a) 1:0 T2K, 1:1 NOνA ν:$\bar{\nu}$, NH. (b) 1:1 T2K, 1:1 NOνA ν:$\bar{\nu}$, NH. (c) 1:0 T2K, 1:1 NOνA ν:$\bar{\nu}$, IH. (d) 1:1 T2K, 1:1 NOνA ν:$\bar{\nu}$, IH.

greater than 50%. Figure 25 shows the summary for median $\Delta\chi^2$ for $\sin\delta_{CP} = 0$. T2K run ratios between 1:0 and 5:5 produce relatively similar values of median $\Delta\chi^2$ for the combined fit. This is also true for combined T2K + NOνA running independent of the NOνA run plan optimization. There is a slight preference for all neutrino running in T2K in the combined fit.

Figures 26 and 27 summarize the δ_{CP} 1 σ width at various values of δ_{CP}. Again, relatively similar values of δ_{CP} 1 σ width are expected for the T2K run ratios between 1:0 and 1:9.

All of the metrics demonstrate a relatively flat response between approximately 7:3 and 3:7 for T2K and for T2K + NOνA(5:5) with systematics, with a worse response outside that range. These results are consistent with several other studies not shown in this paper (e.g. the measures of the precision on $\sin^2\theta_{13}$ in ν-mode and in $\bar{\nu}$-mode). The results are also robust with respect to reasonable variations in $\sin^2\theta_{23}$, δ_{CP}, and the MH. Thus, the results suggest that T2K run with a ν-mode to $\bar{\nu}$-mode at ratio of 1:1 with an allowed variation of $\pm$20% of the total exposure. The variation can be used to

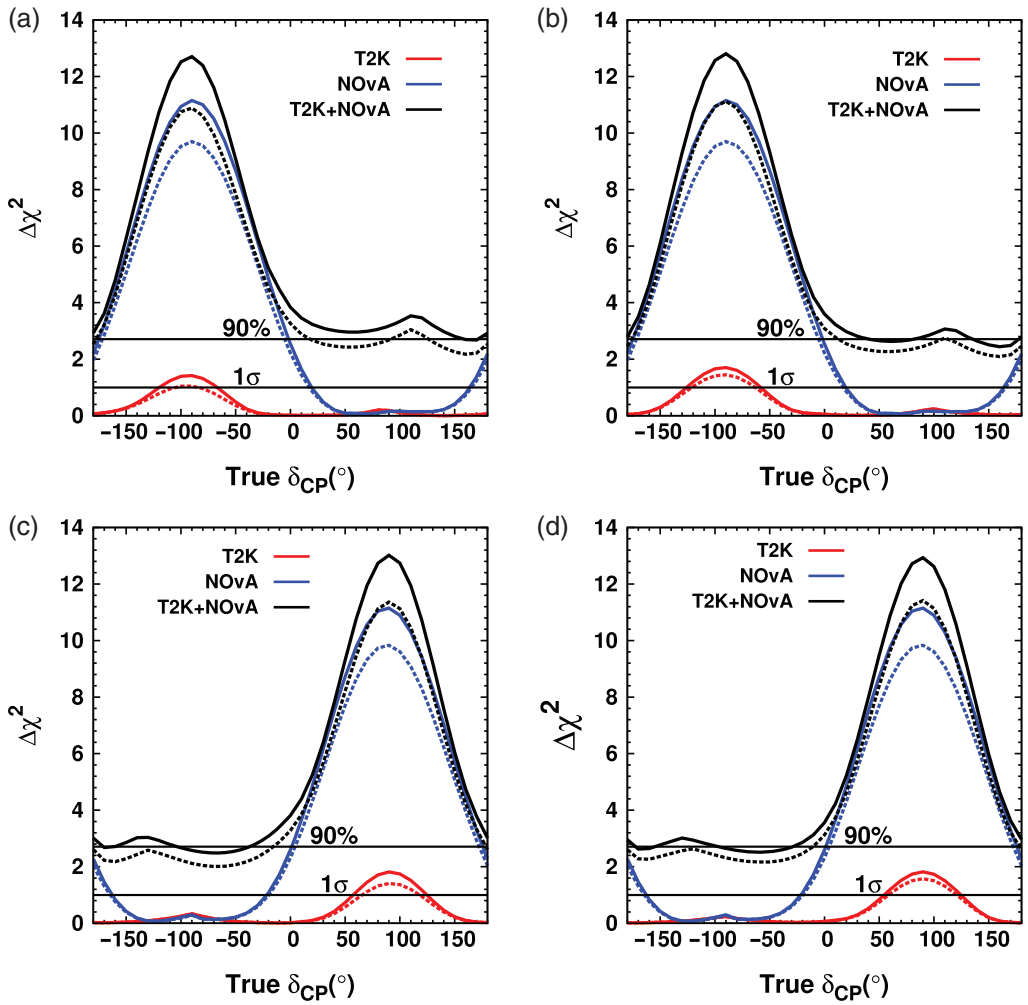

Fig. 21. The predicted $\Delta\chi^2$ for rejecting the incorrect MH hypothesis, as a function of δ_{CP} for T2K (red), NOνA (blue), and T2K + NOνA (black). Dashed (solid) curves indicate studies where normalization systematics are (not) considered. The "true" value of $\sin^2(\theta_{23})$ is assumed to be 0.5, and the "true" MH is assumed to be the NH (top) or the IH (bottom). The "test" MH is unconstrained. (a) 1:0 T2K, 1:1 NOνA ν:$\bar{\nu}$, NH. (b) 1:1 T2K, 1:1 NOνA ν:$\bar{\nu}$, NH. (c) 1:0 T2K, 1:1 NOνA ν:$\bar{\nu}$, IH. (d) 1:1 T2K, 1:1 NOνA ν:$\bar{\nu}$, IH.

optimize the experiment to any one analysis without significant degradation of the sensitivity to any other analysis. A more detailed optimization of the ν:$\bar{\nu}$ run ratio will require tighter constraints on oscillation parameters from future analyses, a more detailed treatment of systematic uncertainties from both T2K and NOνA, and a clear prioritization of analysis goals from the T2K and NOνA collaborations.

7. Summary

In this paper we have presented studies of the T2K experiment sensitivity to oscillation parameters by performing a three-flavor analysis combining appearance and disappearance, for both ν-mode and $\bar{\nu}$-mode, assuming the expected full statistics of 7.8×10^{21} POT. The T2K precision study includes either statistical errors only, systematic errors established for the 2012 oscillation analyses, or conservatively projected systematic errors, and takes into consideration signal efficiency and background. We have derived the sensitivity to the oscillation parameters $\sin^2 2\theta_{13}$, δ_{CP}, $\sin^2 2\theta_{23}$, and Δm^2_{32} for a range of the true parameter values and using constraints from other experiments. For example,

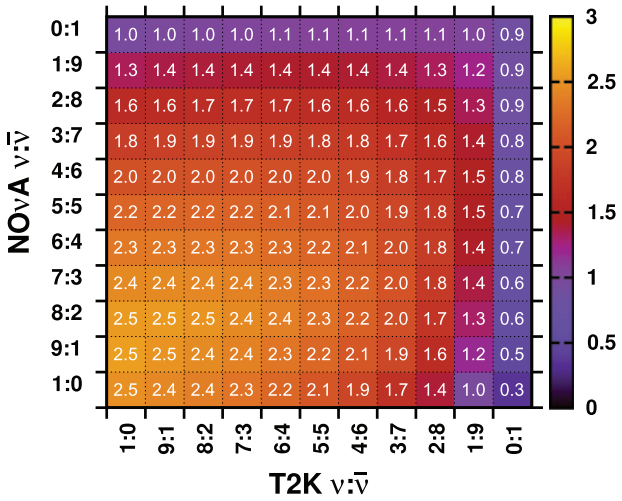

Fig. 22. Lowest $\Delta\chi^2$ for a combined T2K + NOνA fit to determine the mass hierarchy for various ν:$\bar{\nu}$ running ratios. True values are assumed to be: MH=NH, $\sin^2(\theta_{23}) = 0.5$. Normalization systematics are assumed.

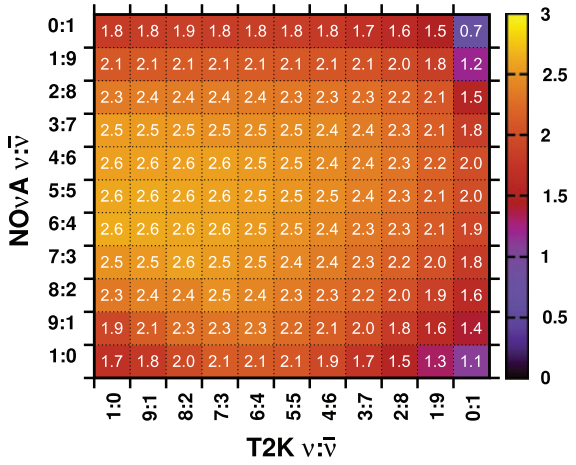

Fig. 23. Median $\Delta\chi^2$ for $\sin\delta_{CP} = 0$ for a combined T2K + NOνA fit. True values are assumed to be: MH=NH, $\sin^2(\theta_{23}) = 0.5$. Normalization systematics are assumed.

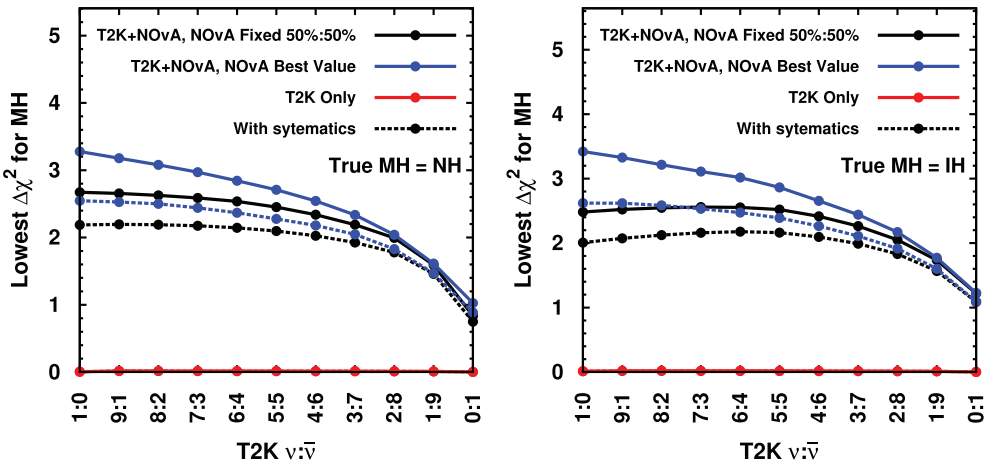

Fig. 24. Lowest $\Delta\chi^2$ for mass hierarchy determination in a combined, T2K + NOνA, fit as a function of T2K ν:$\bar{\nu}$ running ratio for true MH=NH (left) and IH (right). Curves are given for the $\Delta\chi^2$ value at nominal 5:5 NOνA running (black), best case T2K + NOνA running (blue), and T2K-only running (red). Dashed (solid) curves indicate studies performed (without) assuming normalization systematics.

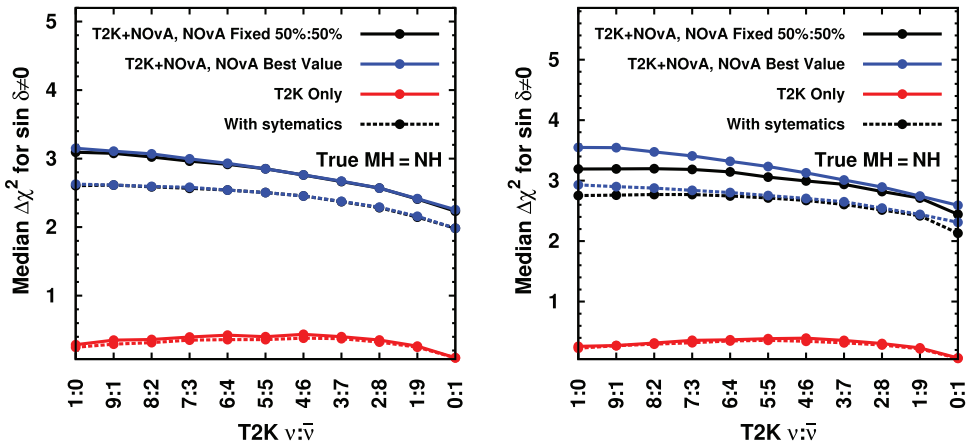

Fig. 25. Median $\Delta\chi^2$ for $\sin\delta_{CP} = 0$ in a combined, T2K + NOνA, fit as a function of T2K ν:$\bar{\nu}$ running ratio for true MH=NH (left) and IH (right). Curves are given for the $\Delta\chi^2$ value at nominal 5:5 NOνA running (black), best case T2K + NOνA running (blue), and T2K-only running (red). Dashed (solid) curves indicate studies performed (without) assuming normalization systematics.

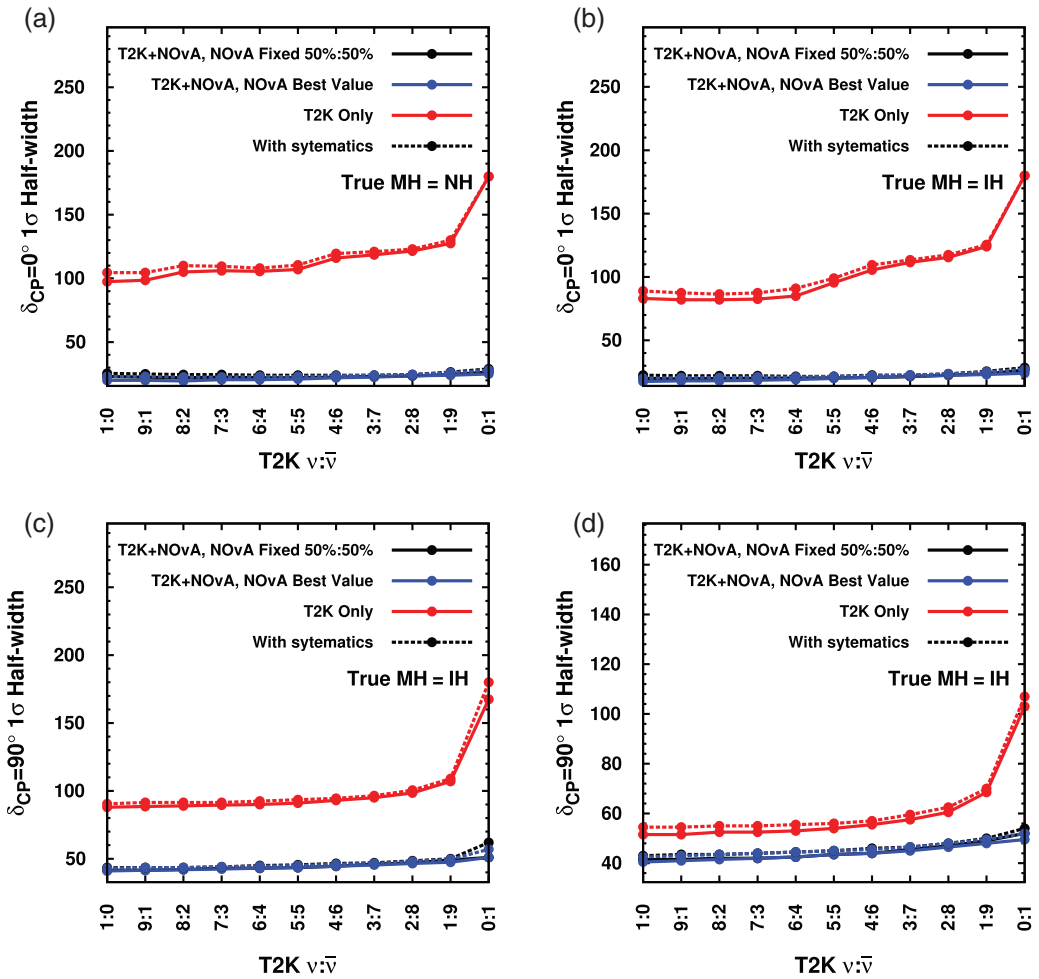

Fig. 26. δ_{CP} resolution in a combined, T2K + NOνA, fit as a function of T2K ν:$\bar{\nu}$ running ratio. Curves are given for the resolution value, in degrees, at nominal 5:5 NOνA running (black), best case T2K + NOνA running (blue), and T2K-only running (red). Dashed (solid) curves indicate studies performed (without) assuming normalization systematics. (a) $\delta = 0°$, NH. (b) $\delta = 0°$, IH. (c) $\delta = 0°$, NH. (d) $\delta = 0°$, IH.

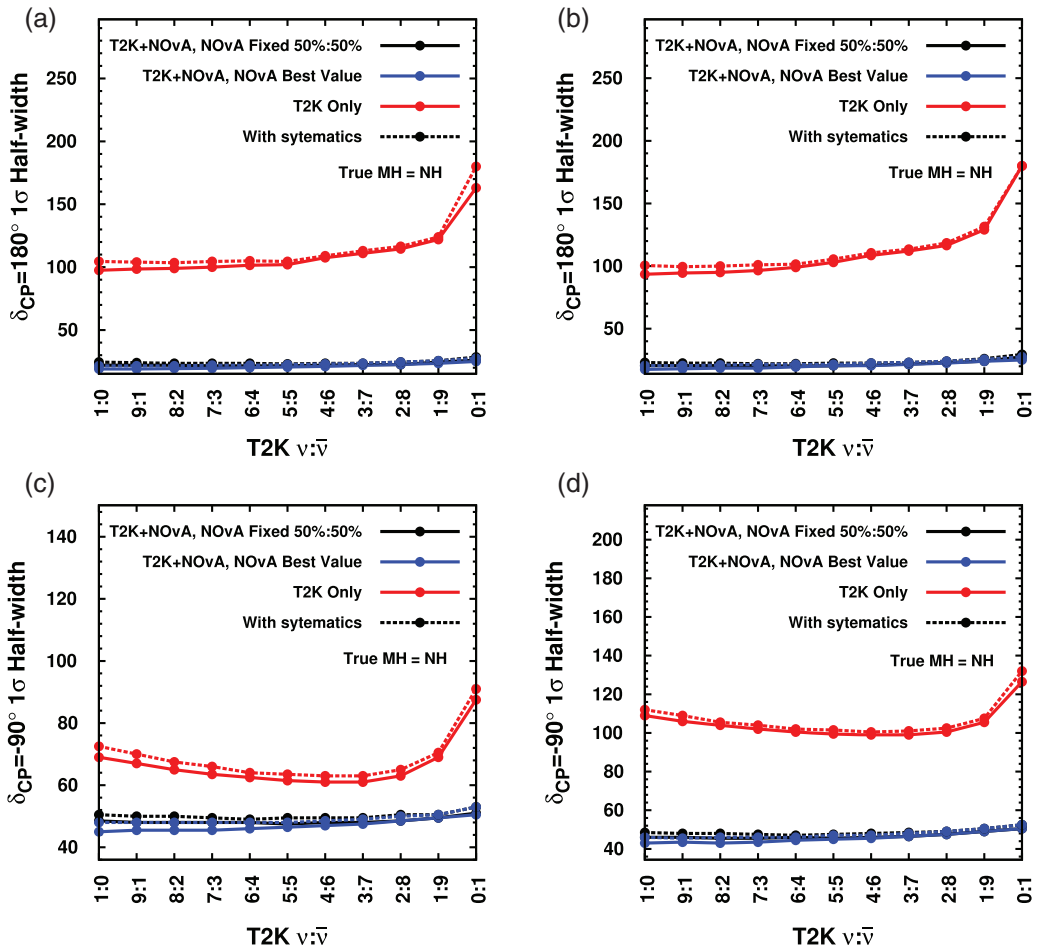

Fig. 27. As Fig. 26, but for different δ_{CP} values. (a) $\delta = 180°$, NH. (b) $\delta = 180°$, IH. (c) $\delta = -90°$, NH. (d) $\delta = -90°$, IH.

with equal exposure of ν-mode and $\bar{\nu}$-mode and using signal efficiency from the 2012 analysis we project a data set of approximately 100 ν_e and 25 $\bar{\nu_e}$ appearance events and 390 (270) ν_μ and 130 (70) $\bar{\nu_\mu}$ CCQE (CC non-QE) events. From these data, with the projected systematic uncertainties we would achieve a 1 σ resolution of 0.050 (0.054) on $\sin^2\theta_{23}$ and 0.040 (0.045) $\times 10^{-3}$ eV^2 on Δm^2_{32} for 100% (50%) neutrino beam mode running. T2K will also have sensitivity to the CP-violating phase δ_{CP} at 90% C.L. or higher over a significant range. For example, if $\sin^2\theta_{23}$ is maximal (i.e. $\theta_{23} = 45°$) the range is $-115° < \delta_{CP} < -60°$ for normal hierarchy and $+50° < \delta_{CP} < +130°$ for inverted hierarchy.

Since the ability of T2K to measure the value of δ_{CP} is greatly enhanced by the knowledge of the mass hierarchy we have also incorporated the expected data from the NOνA experiment into our projections using the GLoBES tools. With the same normalization uncertainties of 5% on the signal and 10% on the background for both experiments we find, for example, that the predicted $\Delta\chi^2$ for rejecting the $\delta_{CP} = 0$ hypothesis for $\delta_{CP} = +90°$, IH, and $\sin^2\theta_{23} = 0.5$ from the combined experiment fit is 8.2 compared to 4.3 and 3.2 for T2K and NOνA alone, respectively. The region of oscillation parameter space where there is sensitivity to observe a non-zero δ_{CP} is substantially increased compared to if each experiment is analyzed alone.

From the investigation of dividing the running time between ν- and $\bar{\nu}$-modes we found that an even split gives the best sensitivity for a wider region of the oscillation parameter space for both T2K data

alone, and for T2K data in combination with NOνA, though the dependence on the ratio is not strong.

It is anticipated that the results of these studies will help to guide the optimization of the future run plan for T2K.

Acknowledgment

We thank the J-PARC staff for superb accelerator performance and the CERN NA61 collaboration for providing valuable particle production data. We acknowledge the support of MEXT, Japan; NSERC, NRC, and CFI, Canada; CEA and CNRS/IN2P3, France; DFG, Germany; INFN, Italy; National Science Centre (NCN), Poland; RAS, RFBR, and MES, Russia; MICINN and CPAN, Spain; SNSF and SER, Switzerland; STFC, UK; and DOE, USA. We also thank CERN for the UA1/NOMAD magnet, DESY for the HERA-B magnet mover system, NII for SINET4, the WestGrid and SciNet consortia in Compute Canada, GridPP, UK. In addition, participation of individual researchers and institutions has been further supported by funds from: ERC (FP7), EU; JSPS, Japan; Royal Society, UK; DOE Early Career program, USA.

Funding

Open Access funding: SCOAP[3].

References

[1] Y. Fukuda et al., Phys. Rev. Lett., **81**, 1562 (1998).
[2] B. T. Cleveland, T. Daily, R. Davis. Jr, J. R. Distel, K. Lande, C. K. Lee, P. S. Wildenhain, and J. Ullman, Astrophys. J., **496**, 505 (1998).
[3] K. Abe et al., Phys. Rev. D, **83**, 052010 (2011).
[4] B. Aharmim et al., Phys. Rev. C, **88**, 025501 (2013).
[5] G. Bellini et al., Phys. Rev. Lett., **108**, 051302 (2012).
[6] K. Eguchi et al., Phys. Rev. Lett., **90**, 021802 (2003).
[7] R. Wendell et al., Phys. Rev. D, **81**, 092004 (2010).
[8] P. Adamson et al., Phys. Rev. Lett., **110**, 251801 (2013).
[9] K. Abe et al., Phys. Rev. Lett., **110**, 181802 (2013).
[10] F. P. An et al., Phys. Rev. Lett., **108**, 171803 (2012).
[11] Y. Abe et al., Phys. Rev. D, **86**, 052008 (2012).
[12] J. K. Ahn et al., Phys. Rev. Lett., **108**, 191802 (2012).
[13] M. H. Ahn et al., Phys. Rev. D, **74**, 072003 (2006).
[14] K. Abe et al., Phys. Rev. Lett., **112**, 181801 (2014).
[15] K. Abe et al., Phys. Rev. Lett., **107**, 041801 (2011).
[16] K. Abe et al., Phys. Rev. D, **88**, 032002 (2013).
[17] K. Abe et al., Phys. Rev. Lett., **112**, 061802 (2014).
[18] P. Adamson et al., Phys. Rev. Lett., **110**, 171801 (2013).
[19] N. Agafonova et al., Phys. Lett. B, **691**, 138 (2010).
[20] Z. Maki, M. Nakagawa, and S. Sakata, Prog. Theor. Phys., **28**, 870 (1962).
[21] Letter of intent: Neutrino oscillation experiment at JHF (2003), http://neutrino.kek.jp/jhfnu/loi/loi_JHFcor.pdf.
[22] K. Abe et al., Nucl. Instrum. Methods Phys. Res., Sect. A, **659**, 106 (2011). [See Figure 16 for a schematic diagram of the ND280 detector.]
[23] Noνa Technical Design Report (2007), http://www-nova.fnal.gov/nova_cd2_review/tdr_oct_23/tdr.htm.
[24] J. Arafune, M. Koike, and J Sato, Phys. Rev. D, **56**, 3093 (1997).
[25] J. Beringer et al., Phys. Rev. D, **86**, 010001 (2012).
[26] K. Abe et al., Phys. Rev. D, **87**, 012001 (2013).
[27] K. Abe et al., Nucl. Instrum. Methods Phys. Res., Sect. A, **694**, 211 (2012).
[28] S. Assylbekov et al., Nucl. Instrum. Meth. A, **686**, 48 (2012).
[29] N. Abgrall et al., Nucl. Instrum. Methods Phys. Res., Sect. A, **637**, 25 (2011).
[30] P. A. Amaudruz et al., Nucl. Instrum. Methods Phys. Res., Sect. A, **696**, 1 (2012).
[31] S. Aoki et al., Nucl. Instrum. Meth. A, **698**, 135 (2013).

[32] Y. Ashie et al., Phys. Rev. D, **71**, 112005 (2005).
[33] N. Abgrall et al., Phys. Rev. C, **84**, 034604 (2011).
[34] N. Abgrall et al., Phys. Rev. C, **85**, 035210 (2012).
[35] K. Abe et al., Phys. Rev. D, **85**, 031103 (2012).
[36] J. Beringer et al., (Particle Data Group), Phys. Rev. D, **86**, 010001, (2012).
[37] F. P. An et al., Chinese Physics C, **37**, 011001 (2013).
[38] P. Huber, M. Lindner, and W. Winter, Comput. Phys. Commun., **167**, 195 (2005).
[39] P. Huber, J. Kopp, M. Lindner, M. Rolinec, and W. Winter, Comput. Phys. Commun., **177**, 432 (2007).
[40] X. Qian, A. Tan, W. Wang, J. J. Ling, R. D. McKeown, and C. Zhang, Phys. Rev. D, **86**, 113011 (2012).